QUARTERLY JOURNAL OF THE ROYAL METEOROLOGICAL SOCIETY
*Q. J. R. Meteorol. Soc.* **135**: 1–19 (2009)
Published online 21 January 2009 in Wiley InterScience
(www.interscience.wiley.com) DOI: 10.1002/qj.351

# Synoptic scale wave breaking and its potential to drive NAO-like circulation dipoles: A simplified GCM approach

Torben Kunz* and Klaus Fraedrich and Frank Lunkeit
*Meteorologisches Institut, Universität Hamburg, Bundesstraße 55, D-20146 Hamburg, Germany*

**ABSTRACT:** Recent studies suggest a synoptic view of the North Atlantic oscillation (NAO) with its positive (negative) phase being the remnant of anticyclonic (cyclonic) synoptic scale wave breaking. This study examines the potential of anticyclonic (AB) and cyclonic wave breaking (CB) to drive NAO-like meridional circulation dipoles by investigating the synoptic evolution of AB and CB events in a mid-latitude eddy-driven jet in a simplified GCM with zonally uniform basic state. First, a method for the detection of such events from daily isentropic maps of potential vorticity and horizontal deformation is constructed. Then, from the obtained sample of events AB- and CB-composites of the upper and lower tropospheric flow are computed, and a distinct spatial and temporal asymmetry in the response to AB and CB events is found. While from the interaction of two AB events (with a mean lifetime of 2.6 days) a strong and short-lived positive phase NAO-like dipole is produced at the surface but not at upper levels, single CB events (4.3 days) are found to drive a strong and more persistent negative phase NAO-like dipole at upper levels but not at the surface. It is concluded that AB (CB) is not capable of driving a positive (negative) phase NAO-like dipole individually. However, the results suggest that equivalent barotropic NAO-like variability may arise from the successive occurrence of AB and CB events. Further, a sensitivity to the strength of the stratospheric polar vortex is found with more (less) frequent AB (CB) events under strong vortex conditions. Copyright © 2009 Royal Meteorological Society

KEY WORDS Rossby wave breaking; Eddy-driven jet; North Atlantic Oscillation

*Received 13 February 2008; Revised 26 September 2008; Accepted 24 October 2008*

## 1. Introduction

The North Atlantic oscillation (NAO) is the dominant mode of low-frequency variability (time scales of 10 days and longer) over the North Atlantic in winter, and accounts for a significant fraction of variance of European climate and weather (Hurrell, 1995; Hurrell *et al.*, 2003). Although the NAO has significant variability on inter-annual and longer time scales it has been shown that its intrinsic time scale is of the order of 10 days (Feldstein, 2000, 2003), in the sense of both composite positive/negative phase NAO events and the autocorrelation *e*-folding time scale of a daily NAO index. Consistently, the NAO is driven, to a large extent, by high-frequency eddy fluxes, though also low-frequency eddies contribute to its growth and decay (e.g., Feldstein, 2003). Nonetheless, other factors of much longer time scales such as sea surface temperatures, tropical variability and influences from the stratosphere play a role for inter-annual variability (Hurrell *et al.*, 2003).

In the simplest picture, the dynamical process that drives the different phases of the NAO, that is, a meridional circulation dipole of opposite vorticity anomalies appears to be fluctuating meridional eddy vorticity fluxes by mid-latitude synoptic scale waves. A simple and illustrative model of this mechanism is presented by Vallis *et al.* (2004), where high-frequency eddy vorticity fluxes are parameterized by stochastic forcing of the barotropic vorticity equation in a mid-latitude band and which locally results in NAO-like meridional circulation dipoles. Although this model captures the dynamical essence of NAO-like variability, it is, certainly, only a crude approximation to the real atmosphere where a large contribution to eddy vorticity fluxes comes from meridional wave propagation during the decay stage of baroclinic waves, characterized by the occurrence of synoptic scale wave breaking (Rivière and Orlanski, 2007). From the synoptic view point of Benedict *et al.* (2004), Franzke *et al.* (2004) and Rivière and Orlanski (2007), accounting for the much more complex nature of the real atmosphere, it is suggested that the positive phase NAO emerges from anticyclonic synoptic scale wave breaking over North America and the North Atlantic, while the negative phase NAO arises from cyclonic wave breaking over the North Atlantic (anticyclonic and cyclonic wave breaking, as in the LC1 and LC2 idealized baroclinic wave life cycles, respectively; see, e.g., Thorncroft *et al.*, 1993.). Woollings *et al.* (2008) give a different interpretation of the positive (negative) phase NAO being driven by less (more) frequent wave breaking at the tropopause.

These studies suggest that the two kinds of synoptic scale wave breaking are capable of driving NAO-like

*Correspondence to: Torben Kunz, Meteorologisches Institut, Universität Hamburg, Bundesstraße 55, D-20146 Hamburg, Germany.
E-mail: torben.kunz@zmaw.de

meridional circulation dipoles of opposite sign. In this context it is reasonable to ask whether additional factors, such as a zonally non-uniform background flow, sea surface temperatures or even tropical influences, are necessary for such wave breaking to merge in a pattern of either phase of the NAO. Although the observed variability, structure and location of the NAO is, to some extent, accounted for by such additional factors, it is suggested by the above studies that its essential dynamics is given by synoptic scale wave breaking processes – and, thus, might be contained in a flow with zonally uniform basic state. To test this hypothesis the present study addresses the following central question: *Does anticyclonic (cyclonic) wave breaking alone result in positive (negative) phase NAO-like circulation dipoles?* To approach this issue a set of forced-dissipative simulations of a mid-latitude eddy-driven jet is carried out with a simplified GCM, using a zonally uniform basic state. In order to investigate the synoptic evolution of both kinds of wave breaking, a method for the detection of such events is first constructed and then applied to the model output.

Consequently, this paper is organized as follows: The model and the specific setup used for this study is described in section 2. The wave breaking detection method is introduced in section 3. Section 4 presents composites of the wave breaking events detected from the model simulations, and also briefly investigates the influence of the strength of the stratospheric polar vortex on tropospheric wave breaking characteristics, since the NAO is known to depend also on stratospheric conditions (e.g., Baldwin *et al.*, 1994). Though a closer treatment of such stratospheric impacts is left to a subsequent study including stationary planetary waves.

## 2. Model and experimental setup

### 2.1. Model

For the numerical experiments of this study we use the dry primitive equation model PUMA (Fraedrich *et al.*, 1998, 2005, model code and users guide are freely available at http://www.mi.uni-hamburg.de/puma). Such simplified general circulation models provide a platform for a systematic analysis of the dynamics of planetary atmospheres under idealized conditions, with minimal computational expenses allowing for sufficiently long model time series for statistical data analysis. Here, we use this model with T42 spectral horizontal resolution, 30 $\sigma$-levels in the vertical, and a timestep of 15 minutes. Nine model levels are located in the troposphere (equally spaced w.r.t. $\sigma$) and 21 levels above (equally spaced w.r.t. $\ln\sigma$) with the uppermost model level at about 112 km (as in Scinocca and Haynes, 1998, see their Appendix, but with $\sigma_{\mathrm{tran}} = 0.223$). Diabatic heating is represented by Newtonian relaxation towards an equilibrium temperature with heating timescales of 5, 10, 15, 20, and 30 days on the five lowermost model levels, respectively, and 40 days above. Rayleigh friction is applied to the three lowermost model levels to account for frictional effects in the planetary boundary layer with damping timescales of 1.168, 1.759, and 3.562 days, corresponding to the Held and Suarez (1994) scheme. Further, a sponge layer is introduced by applying Rayleigh friction to all levels above 0.5 hPa (as in Polvani and Kushner, 2002, see their Appendix) to avoid spurious wave reflection at the model top and numerical instability due to large amplitude gravity waves. Finally, the model employs horizontal 8th-order ($\nabla^8$) hyperdiffusion with a dissipation timescale of 6 hours on the smallest resolved scale.

### 2.2. Experimental Setup

Since this study focuses on the effect of synoptic scale wave breaking processes on the large scale flow in a zonally uniform setup, we integrate the model with zonally uniform forcing and boundary conditions to avoid any explicit forcing of stationary planetary waves. The dynamical fields of the simulations are, therefore, statistically independent of longitude. Four different simulations are carried out which differ only in the diabatic forcing in terms of the equilibrium temperature in the winter polar stratosphere above 100 hPa. The strength of the polar vortex is controlled by changing the vertical lapse rate $\gamma$ in that region (see the Appendix for an exact specification of the equilibrium temperature). One simulation is performed with no polar vortex (Sim-0) and three further simulations with weak (Sim-1), medium (Sim-2) and strong (Sim-3) vortex forcing, where $\gamma = 0$, 1, 2, 3 K/km, respectively. All other parameters are kept fixed. The forcing is time-independent and represents perpetual northern winter conditions. For each simulation the model is integrated over 30 years (10800 days) and the initial five years are discarded to exclude effects from the model's spin-up phase.

Figure 1 shows the different equilibrium temperatures together with the corresponding time and zonal mean zonal winds of the respective simulations. Clearly, the strengthened stratospheric polar vortex is the main response to increased high-latitude stratospheric cooling. However, there are also changes in the tropospheric circulation, specifically, a slight poleward shift of the mid-latitude eddy-driven jet. This tropospheric response resembles that found by Polvani and Kushner (2002) and Kushner and Polvani (2004), using a similar model and setup, and where it is suggested that a baroclinic response in the troposphere essentially accounts for those changes. Our choice of the tropospheric and lower stratospheric forcing, however, differs from those studies in the sense that it always produces an eddy-driven jet at mid-latitudes, which is more suggestive of the dynamical state over the North Atlantic in winter, compared to a jet at 30 °N in the North Pacific sector. Moreover, the latitudinal shift of the simulated jet (from 46 °N in Sim-0 to 49 °N in Sim-3) compares well with the change in latitude of the observed eddy-driven jet over the North Atlantic, associated with the NAO (for reference see, e.g., Ambaum *et al.*, 2001, their Fig. 7). Recalling the conceptual background of this study, namely the investigation



DOI: 10.1002/qj

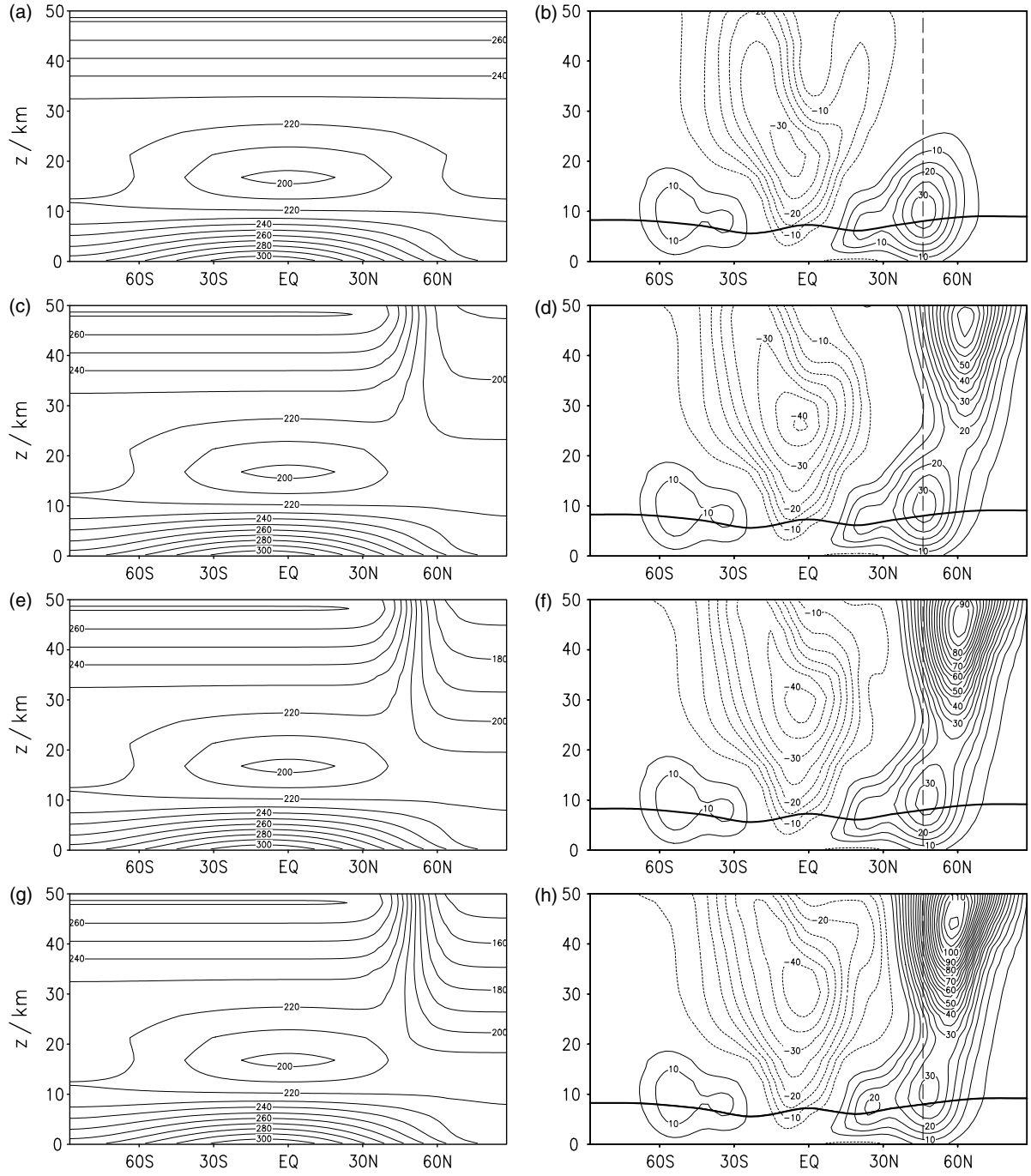


Figure 1. Equilibrium temperature (in K, left) and zonally and time averaged zonal winds (in $ms^{-1}$, right) of the simulations with no (Sim-0), weak (Sim-1), medium (Sim-2) and strong (Sim-3) stratospheric polar vortex (from top to bottom; using the last 25 years each). Zonal winds are shown together with the $\theta = 320\,K$ surface (thick line); and the thin dashed vertical line marks 46 °N. Only the lower part of the model domain is shown.

of the relevance of synoptic scale wave breaking for the NAO, this appears as one advantage of the configuration of our forcing. Finally, the subtropical jet at the edge of the Hadley cell is weak compared to the real atmosphere, as it is often the case for simplified dry general circulation models due to the lack of tropical moist convective variability. Hence, this model setup is optimal for the study of extratropical synoptic scale wave breaking in a mid-latitude eddy-driven jet, excluding potential external factors like tropical variability, sea surface temperatures or ultralong (wavenumber 1 to 3) quasi-stationary planetary waves.

## 3. Wave breaking detection method

The concept of Rossby wave breaking (McIntyre and Palmer, 1983, 1985) was first applied to ultralong planetary waves in the winter stratosphere. However, many studies are also concerned with breaking synoptic scale Rossby waves near the tropopause during their barotropic



DOI: 10.1002/qj

decay stage, and its dynamical relevance for the large scale tropospheric circulation (e.g., Thorncroft *et al.*, 1993; Nakamura and Plumb, 1994; Peters and Waugh, 1996; Esler and Haynes, 1999; Benedict *et al.*, 2004; Abatzoglou and Magnusdottir, 2006; Martius *et al.*, 2007; Woollings *et al.*, 2008), or mass/tracer transport between the stratosphere and troposphere (e.g., Appenzeller and Davies, 1992; Waugh *et al.*, 1994). Rossby wave propagation ultimatively originates from background potential vorticity (PV) gradients which provide the restoring force for the associated parcel oscillations. When such waves attain large amplitudes non-linear advection processes come into play, leading to large horizontal parcel displacements and, eventually, to irreversible mixing of PV. This can be seen best in the large scale overturning of isentropic PV contours near the tropopause, indicating a local reversal of the PV gradient and, therefore, inhibiting further Rossby wave propagation in that region. This reversed PV gradient is the essential dynamical aspect of breaking Rossby waves, and, therefore, has been used in different studies for their detection (e.g., Abatzoglou and Magnusdottir, 2006; Woollings *et al.*, 2008). Our wave breaking detection method is also based on this idea and introduced in the following subsection together with a kinematic criterion for classification into anticyclonically and cyclonically breaking waves.

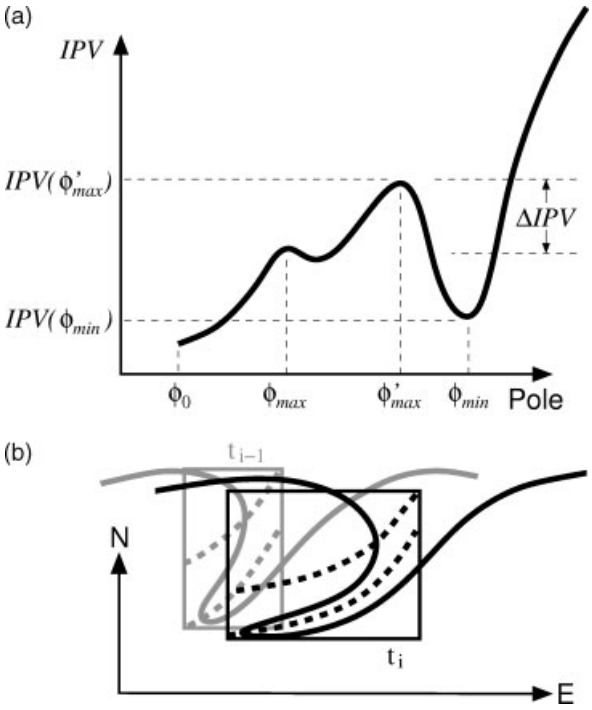


Figure 2. Wave breaking detection method (schematics). (a) Detection of an $IPV$ reversal. The thick line indicates the meridional $IPV$ profile at a given longitude. See text for an explanation of symbols. (b) Wave breaking region and tracking in time. Thick solid lines indicate $IPV$ contours on day $t_i$ (black) and on the previous day $t_{i-1}$ (gray). Dashed lines represent the trough (at $\phi'_{max}$) and ridge axis (at $\phi_{min}$). The respective wave breaking regions are marked by rectangles.

### 3.1. Detection of a breaking wave

The method for the detection of breaking synoptic scale Rossby waves in the troposphere used in this model study works as follows. First, daily isentropic maps of Ertel's PV (*IPV* maps for short) on an upper tropospheric isentropic surface are calculated, poleward of 20° latitude in the winter hemisphere. We choose the $\theta = 320\,K$ potential temperature surface, which is located between 400 hPa and 350 hPa in the tropics and around 270 hPa at polar latitudes for this model setup (see Fig. 1). Then, on this $\theta$-surface an individual wave breaking event is, basically, defined as a two-dimensional horizontal structure characterized by a reversed (i.e., negative) meridional $IPV$ gradient, and is detected and tracked in time by the following three steps:

*Step 1 (search for meridional IPV reversal).* At each longitude (of the corresponding Gaussian model grid with 128 longitudes at T42) the meridional $IPV$ profile is searched for reversals of the poleward $IPV$ gradient from positive to negative values. Specifically (see Fig. 2a for illustration), starting from $\phi_0 = 20\,^{\circ}\mathrm{N}$, the method looks for the latitude $\phi_{max}$ of the first $IPV$ maximum $IPV(\phi_{max})$. Next, if $\phi_{max} < 90\,^{\circ}\mathrm{N}$, the absolute $IPV$ minimum north of $\phi_{max}$ is searched, located at $\phi_{min}$. Finally, the absolute $IPV$ maximum between $\phi_{min}$ and $\phi_{max}$ is determined, $IPV(\phi'_{max})$. Now, if

$$IPV(\phi'_{max}) - IPV(\phi_{min}) > \Delta IPV, \qquad (1)$$

with a prescribed threshold value $\Delta IPV$, then this $IPV$ reversal is said to belong to a wave breaking event. If condition (1) is true for $\Delta IPV = \Delta IPV_{detect} = 1$ PVU, it is called a strong reversal, if (1) is true only for $\Delta IPV = \Delta IPV_{extend} = 0.75$ PVU it is called a weak reversal (where 1 PVU = 1 potential vorticity unit $= 10^{-6} s^{-1}\mathrm{Km^2kg^{-1}}$). $\phi'_{max}$ and $\phi_{min}$ are the southern and northern bounds, respectively, of this wave breaking event at the particular longitude, and correspond to the latitude of the associated $IPV$ trough and ridge, respectively. Subsequently, the same longitude is searched for further $IPV$ reversals at higher latitudes by iteration of step 1, starting from the northern bound of the previously detected reversal, say, with $\phi_0 = \phi_{min}$.

*Step 2 (longitudinal extension).* Different $IPV$ reversals found by step 1, which occur at neighboring longitudes $\lambda$, are grouped together and taken as the same wave breaking event, if the difference in their latitudinal position in terms of $\phi_{max}$ is less than two gridpoints ($\sim 5^{\circ}$ latitude at T42), and if at least one strong reversal is contained in this group. Note, that with $\Delta IPV_{detect}$ (1) becomes the necessary condition for detection of an event, while with $\Delta IPV_{extend}$ (1) becomes a sufficient condition for longitudinal extension of an event. Now, individual wave breaking events consist of two-dimensional horizontal $IPV$ structures, characterized by an $IPV$ trough-ridge-pair with anticyclonic $IPV$ north of cyclonic $IPV$; and the wave breaking region is defined as the area within the longitude-latitude box spanned by the westernmost and easternmost longitude of the event, and the southernmost point of the $IPV$ trough axis (given by $\phi'_{max}$) and the



DOI: 10.1002/qj

northernmost point of the $IPV$ ridge axis (given by $\phi_{min}$). The central point, $(\lambda_c, \phi_c)$, of an event is defined as the center of its wave breaking region.

*Step 3 (time tracking).* Two wave breaking events found by step 2, which occur on subsequent days, are taken as the same event in case of spatial overlap of their wave breaking regions. See Fig. 2b for an illustration of this tracking in time. Thus, each wave breaking event persists for a certain number of days $N_t$. In order to exclude very short-lived events which only marginally fulfill the conditions for detection, all events with $N_t = 1$ are discarded.

### 3.2. Classification into anticyclonic and cyclonic wave breaking

The method for the detection of wave breaking events also allows for classification into anticyclonic and cyclonic wave breaking. The typical synoptic signature of anticyclonic wave breaking (AB), associated with equatorward wave propagation towards a critical line in the subtropics, is an $IPV$ trough-ridge-pair with a NE-SW tilted trough axis, with a continual thinning and an increasing zonal orientation of the trough with time. Cyclonic wave breaking (CB), on the other hand, is associated with weak poleward wave propagation out of a leaky zonal wave guide, on the poleward flank of the jet. Corresponding synoptic $IPV$ maps show a NW-SE tilted trough during the evolution of a CB event, and this trough becomes broader with time. Since AB (CB) events occur in regions of anticyclonic (cyclonic) zonal wind shear, this behavior of trough thinning (broadening) may be qualitatively understood by simple scale arguments for PV inversion given by Thorncroft *et al.* (1993). Moreover, the above mentioned synoptic evolution during AB implies a pattern of zonal stretching (and meridional contraction) in the region of the PV trough, since PV is nearly conserved in the upper troposphere where diabatic and frictional processes are weak on the synoptic time scale of a few days. An example of an AB event is presented in Fig. 3a, taken from simulation Sim-2. The $IPV$ trough has a clear NE-SW tilt and the zonal orientation of the axis of dilatation indicates zonal stretching. During a typical CB event, on the other hand, we have meridional stretching (and zonal contraction) in the region of the $IPV$ trough, that makes this trough broader with time. The respective example of a CB event (Fig. 3b) exhibits a NW-SE tilted trough and a meridional orientation of the axis of dilatation.

We use these different characteristics of the deformation field to define a kinematic criterion to classify the detected wave breaking events into AB and CB. First, daily maps of isentropic horizontal stretching deformation

$$S = \frac{1}{a\cos\phi}\left(\frac{\partial u}{\partial \lambda} - \frac{\partial}{\partial \phi}(v\cos\phi)\right) \tag{2}$$

are calculated for the same area and level as the $IPV$, where $u$ and $v$ are the isentropic zonal and meridional wind components, respectively, and $a$ the Earth's radius. Positive (negative) $S$ indicates zonal (meridional) stretching. Next, for each individual wave breaking event that occurs on days $t_1, \ldots, t_{N_t}$ the initial stretching $S_1 = S(\lambda_{max}, \phi'_{max}, t_1)$ is determined. Here, $(\lambda_{max}, \phi'_{max})$ is that point on the $IPV$ trough axis with the maximum meridional $IPV$ reversal $IPV(\phi'_{max}) - IPV(\phi_{min})$ (marked by a rectangle in Fig. 3). Then, given a threshold value $S_1^\star$, a wave breaking event may be classified as follows:

$$\text{Event is of type} \begin{cases} \text{AB}, & \text{if} \quad S_1 > S_1^\star \\ \text{CB}, & \text{if} \quad S_1 < S_1^\star \end{cases} . \tag{3}$$

Alternatively, to extract the most distinct AB and CB events from a set of wave breaking events for the computation of AB- and CB-composites, two thresholds

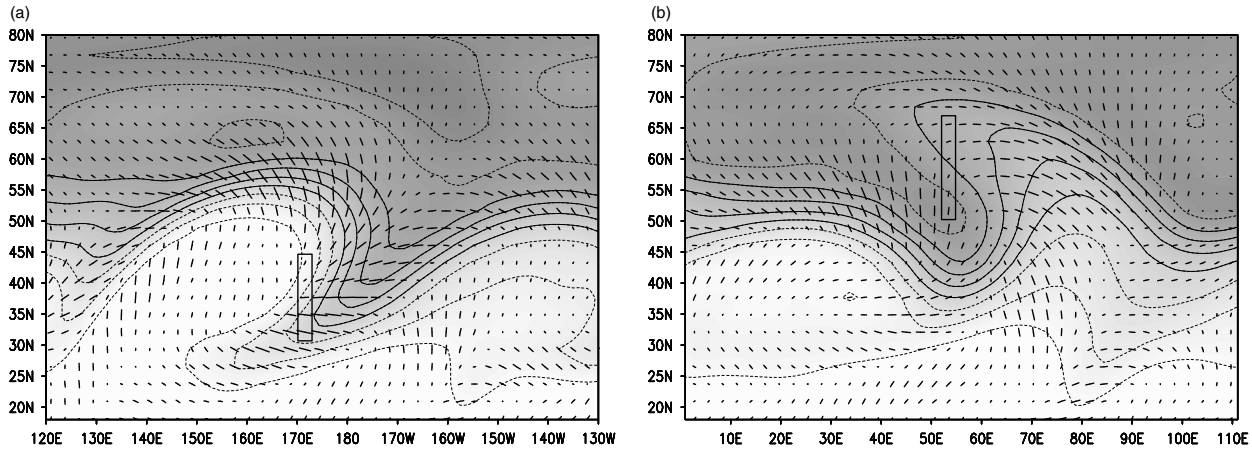


Figure 3. Examples of an anticyclonic (AB, a) and cyclonic wave breaking event (CB, b), detected by the wave breaking detection method on day 2433 and day 7001, respectively, of Sim-2. $IPV$ at $\theta = 320$ K is shown by contours and shading. Contour interval is 0.5 PVU; solid contours are at 2, 2.5, 3 and 3.5 PVU; darker shading represents larger values. Isentropic deformation is depicted by axes of dilatation; length of line segments indicates rate of deformation. Rectangles encircle grid points of the strongest $IPV$ reversal of the respective event, i.e., from $(\lambda_{max}, \phi'_{max})$ to $(\lambda_{max}, \phi_{min})$.



DOI: 10.1002/qj

are defined by the upper ($Q_+$) and lower ($Q_-$) quantiles of the $S_1$ distribution, respectively:

$$\text{Event is used for} \begin{cases} \text{AB-composite,} & \text{if} \quad S_1 > S_1^{Q+} \\ \text{CB-composite,} & \text{if} \quad S_1 < S_1^{Q-} \end{cases} . \tag{4}$$

For the composite analysis in the next section we choose the 15.9%-quantiles and, thus, there are 15.9% of all events with $S_1 > S_1^{Q+}$ and 15.9% with $S_1 < S_1^{Q-}$.

### 3.3. Application of the method

We now apply this method to the four model simulations Sim-0 to Sim-3 (using the last 25 years each). The numbers of detected wave breaking events are listed in Tab. I. There are about a thousand events per simulation and 4119 events total. Thus, on average, one event is detected every 8.7 days; and it has a mean duration of 3.5 days. The time evolution of two examples (same events as in Fig. 3) is illustrated in Fig. 4, where maps are rotated such that, at the time of detection, the breaking wave appears below the center of the respective polar stereographic map. The first case (Fig. 4a) clearly exhibits all features of a typical AB event as described above, and the initial stretching at $(\lambda_{max}, \phi'_{max})$ (marked point in Fig. 4) takes the value $S_1 = 76.0 \times 10^{-6}\text{s}^{-1}$. Note, that in this situation waves show AB-like behavior around the entire hemisphere. In the second case (Fig. 4b), on the other hand, the synoptic signature of a CB event is visible. In particular, three days after the detection an isolated area of low $IPV$ appears at high latitudes. And, on the trough of the breaking wave, the initial stretching $S_1 = -34.6 \times 10^{-6}\text{s}^{-1}$ is obtained. Note, that a few days earlier an AB event occurs about 120° west of the CB event.

Furthermore, the band of steepest $IPV$ gradients indicates the position of the jet since the strongest flow curvature occurs across the jet axis. From this, we find these AB (CB) events to appear on the equatorward (poleward) side of the jet, associated with anticyclonic (cyclonic) shear. Finally, the region between 2 and 3.5 PVU (marked by thick contours in the figure) approximately represents the extratropical tropopause layer for this model setup. Thus, the AB event in Fig. 4a (at +1 day) also shows how isentropic stratosphere-troposphere-exchange comes along with this wave breaking process.

Table I. Numbers of detected wave breaking events $N_{\text{WB}}$ from the four model simulations (using the last 25 years each) and total number; upper and lower 15.9%-quantiles, $S_1^{Q+}$ and $S_1^{Q-}$, respectively, of the corresponding $S_1$ (initial stretching) distributions, in units of $10^{-6}\text{s}^{-1}$.

| Simulation | $N_{\text{WB}}$ | $S_1^{Q+}$ | $S_1^{Q-}$ |
|---|---|---|---|
| Sim-0 | 1102 | 43.5 | −12.5 |
| Sim-1 | 1105 | 52.3 | −12.5 |
| Sim-2 | 910 | 59.8 | −9.8 |
| Sim-3 | 1002 | 54.5 | −7.5 |
| Total | 4119 | - | - |

The frequency distribution of the initial stretching $S_1$ of all 4119 events, shown in Fig. 5a, is suggestive of a bimodal behavior of $S_1$. This bimodality becomes even more evident when the wave breaking detection method is applied to the same data, but with higher detection thresholds, $IPV_{detect} = 1.7$ PVU and $IPV_{extend} = 1.275$ PVU (where, as before, $IPV_{extend} = 0.75 \times IPV_{detect}$), capturing only the strongest events (352 in total). The associated $S_1$ frequency distribution (Fig. 5b) clearly consists of two different modes. From the composites analysed below it becomes obvious that these two modes are associated with anticyclonic and cyclonic wave breaking, confirming the usefulness of the initial stretching $S_1$ for classification into AB and CB. Also the $S_1$ values of the above mentioned two examples of an AB and CB event fall into the opposite sides of the frequency distribution. Note, however, that for all further analysis the low detection thresholds $IPV_{detect} = 1.0$ PVU and $IPV_{extend} = 0.75$ PVU are used to obtain a larger sample of events. Although smaller detection thresholds further increase the sample size, a large number of sub-synoptic scale $IPV$ reversals is then included which are not the focus of this study. Testing different values (not shown) we found the aforementioned detection thresholds to be a reasonable choice.

AB- and CB-composites of $IPV$ are shown in Fig. 6a and b, taken on the first day of each event, shifted in longitude and latitude in a way that the central point $(\lambda_c, \phi_c)$ of each event is located in the center of the map (with relative longitude $\lambda_{rel} = \lambda - \lambda_c$ and latitude $\phi_{rel} = \phi - \phi_c$). Here, the events are classified into AB and CB according to (3), with $S_1^\star = 26 \times 10^{-6}s^{-1}$. This threshold roughly separates the two modes in the $S_1$ frequency distribution. Both, AB- and CB-composites, reveal the typical synoptic signature of a thin NE-SW tilted trough for AB and a broad NW-SE tilted trough for CB with the formation of a cut-off cyclone. These composites are compared to those calculated according to (4), using the 15.9%-quantiles (Fig. 6c, d), and strong similarity between the respective patterns is found. Note, that the quantiles are calculated for each simulation separately, and are listed in Tab. I. The according composites for the separate simulations (not shown) are very similar to the total composites in Fig. 6 which our analysis is, thus, based on. Also for the remaining composite analysis in the next section we only show composites calculated according to (4), since, first, the two modes in the $S_1$ frequency distribution strongly overlap at intermediate values of $S_1$ and, second, the threshold value of $S_1^\star$ is somewhat arbitrary and, therefore, using (4) for composite classification is cleaner. Though, all composites were also calculated using (3) and, qualitatively, the same results are obtained.

## 4. Anticyclonic and cyclonic wave breaking

In this section we extend the previously described composite analysis to gain insight into the synoptic evolution



DOI: 10.1002/qj

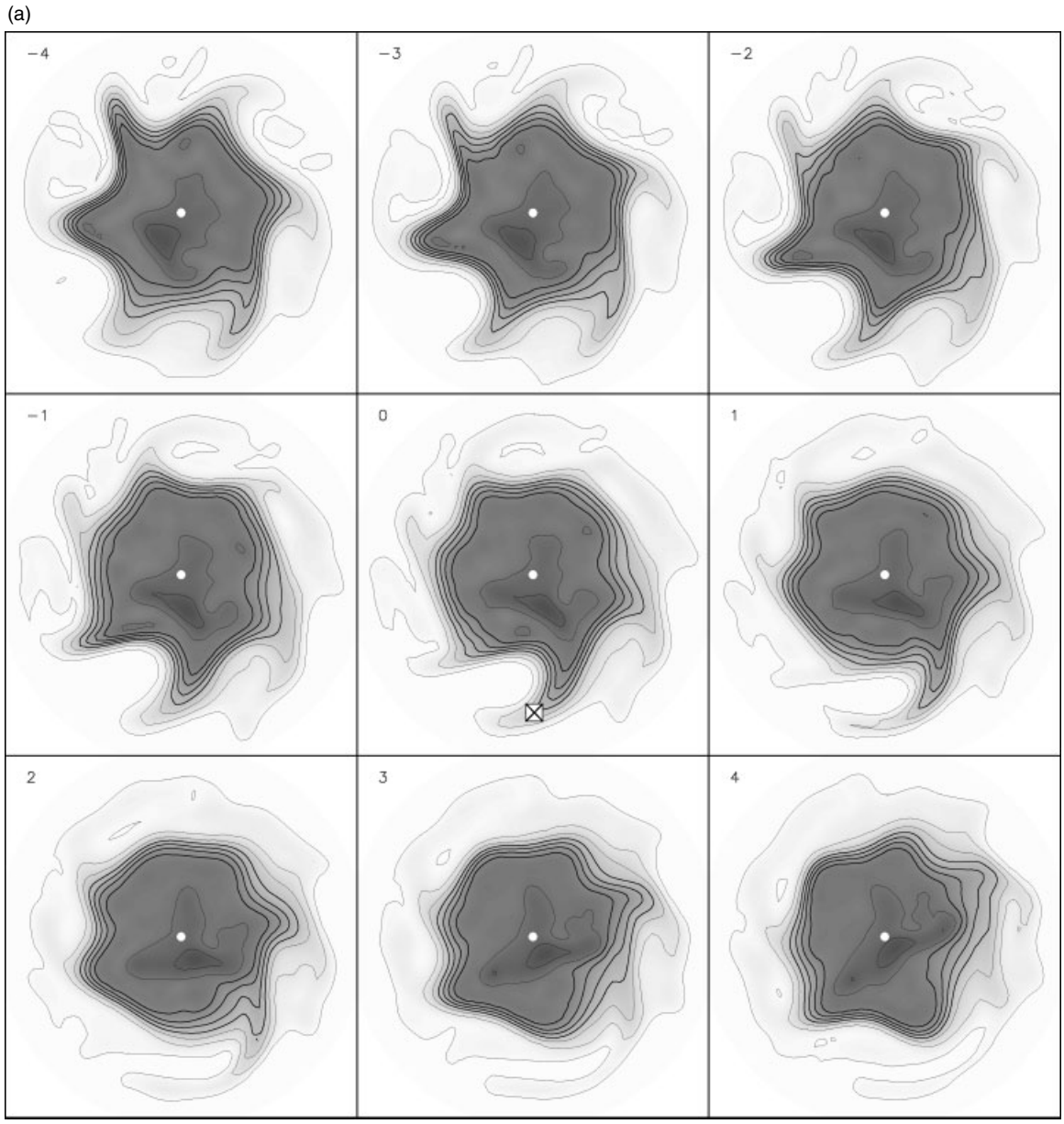


Figure 4. Same examples of an AB (a) and CB event (b) as in Fig. 3. $IPV$ at $\theta = 320$ K (north of 20 °N) is shown by contours and shading. Contour interval is 0.5 PVU; lowest contour is at 0.5 PVU; thick contours are at 2, 2.5, 3 and 3.5 PVU; darker shading represents larger values. Cross symbols mark the point $(\lambda_{max}, \phi'_{max})$ where the initial stretching $S_1$ is evaluated. Numbers are days relative to the time of detection.

of the AB and CB events detected by our method, and to investigate its potential to drive NAO-like meridional dipole patterns. Subsequently, the main results are quantitatively confirmed by studying the impact of the two kinds of wave breaking on the annular mode, that is, the dominant dynamical mode in the model. Finally, at the end of this section, we briefly discuss some differences in the wave breaking statistics among the simulations with different stratospheric forcing.

### 4.1. Synoptic evolution of breaking waves

First, lagged AB- and CB-composites of $IPV$ at $\theta = 320$ K are presented (Fig. 7) to illustrate the temporal evolution of the detected wave breaking event (AB-/ CB-composite classification according to (4), with each composite including 655 events total). Shown are $IPV$ anomalies with respect to the zonal mean at lag -14 days (lag -14 for short) when the respective composites are virtually zonally uniform. Thus, anomalies in Fig. 7 represent the total change in the course of a wave breaking event, including zonal mean changes. As before, composites are shown with relative longitude $\lambda_{rel}$ and latitude $\phi_{rel}$. Each individual relative latitude $\phi_{rel}$ occurs for a certain number of wave breaking events $N(\phi_{rel})$ which can be smaller than the total number of events $N_{tot}$, since for some events a few relative latitudes correspond to absolute latitudes $\phi$ beyond the north pole. Thus, composites are reliable only at those relative latitudes where the ratio $r(\phi_{rel}) = N(\phi_{rel})/N_{tot}$ is close to one, i.e., where a large number of events enter the composite



DOI: 10.1002/qj

(b)

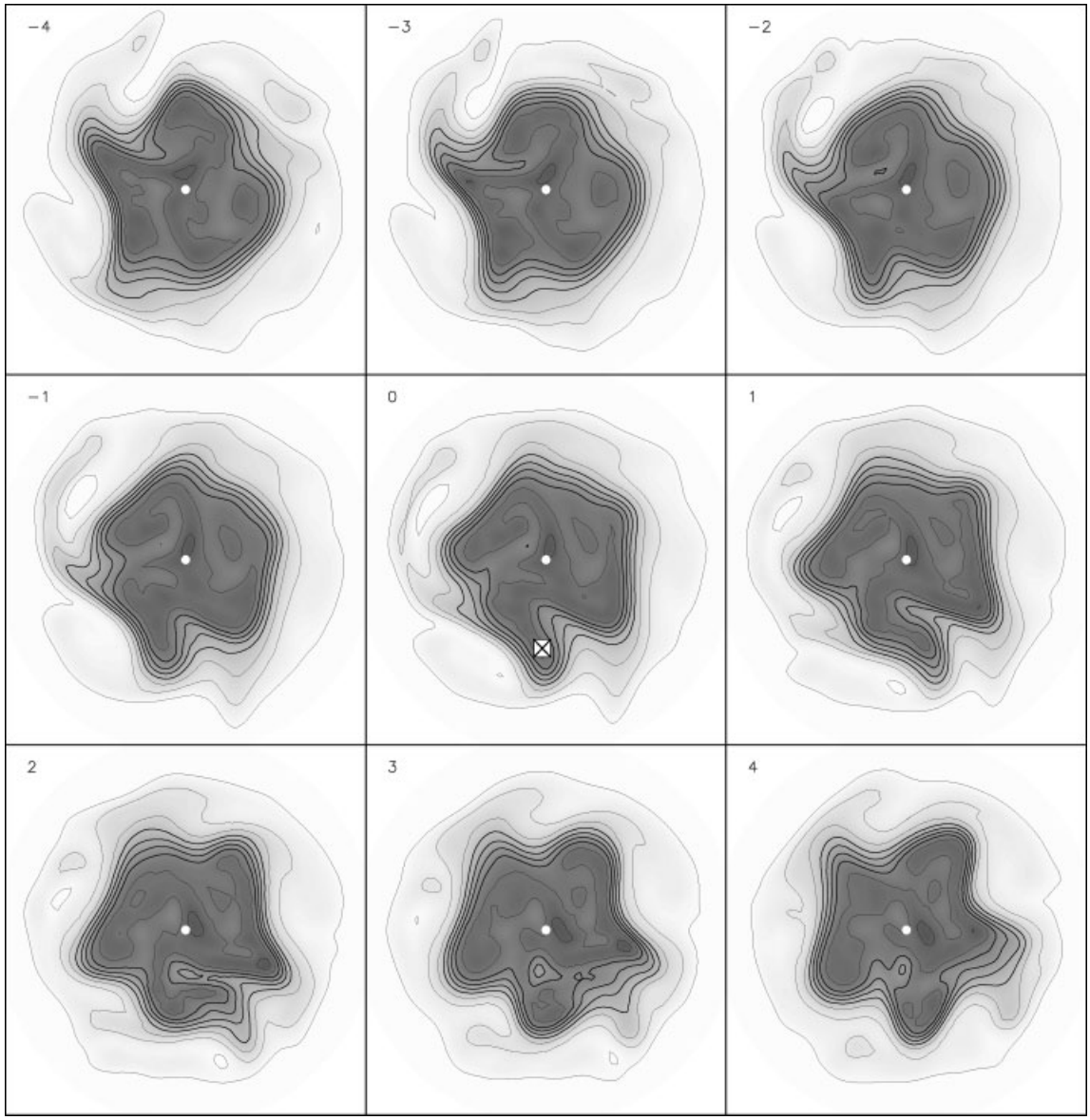


Figure 4. *continued.*

analysis. This ratio is included in Fig. 7 by white (black) shading where $r = 1$ ($r = 0$). The much smaller values of $r$ at high relative latitudes in the CB-composite compared to the AB case clearly indicate the more poleward occurrence of CB events. This is a consequence of the fact that CB events take place on the poleward side and AB events on the equatorward side of the jet.

Both, the AB- and CB-composites show a wave group propagating eastward on the background $IPV$ gradient in the westerly jet, with a clear downstream development signature as it is typical for Rossby waves. Moreover, these wave groups grow in amplitude as lag 0 is approached, as indicated by the increasing isentropic north-south parcel displacement (or $IPV$ contour undulation), and, consequently, the waves become more and more affected by the meridionally varying background flow.

In the AB-composite, under the influence of anticyclonic background shear, the wave group shows equatorward propagation, and, subsequently, the NE-SW tilted $IPV$ trough of the detected wave breaking event becomes zonally stretched and, eventually, quickly dissipates away. From this trough also a small and short-lived cut-off low is produced by lag 2. This is often observed in the real atmosphere as well as in idealized baroclinic wave life cycles during anticyclonic wave breaking events, and frequently initiates cold-frontal cyclogenesis as mentioned by, e.g., Thorncroft *et al.* (1993) and investigated in more detail by Thorncroft and Hoskins (1990). The northern part of this trough, however, travels further downstream along the northern flank of the jet and also quickly dissipates. Note, that all other troughs of this wave group also have a marked NE-SW tilt and thus the waves to the west of the breaking wave undergo an evolution similar to that of the breaking wave itself



DOI: 10.1002/qj

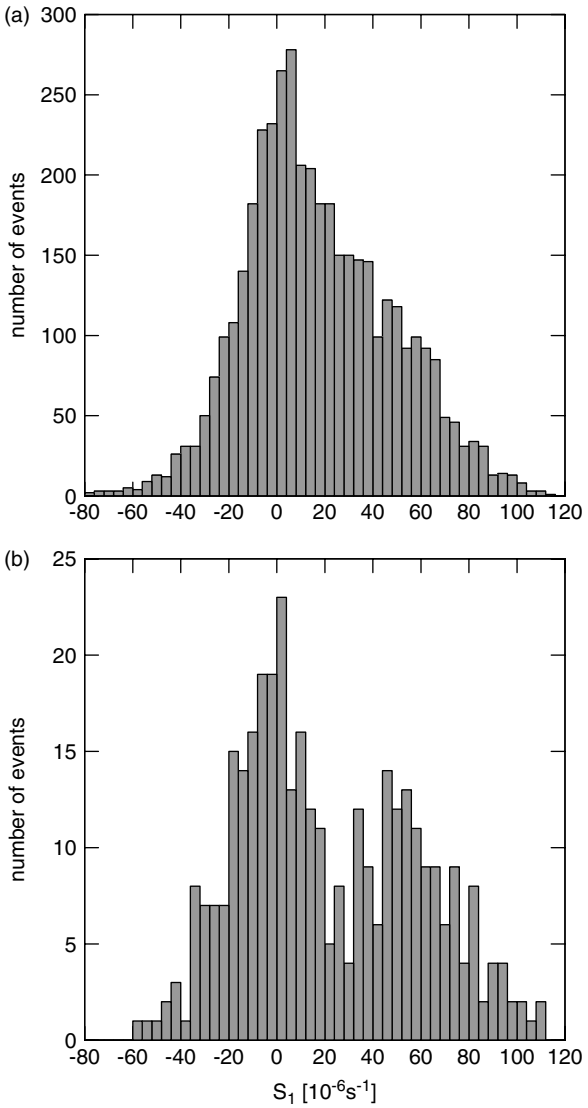


Figure 5. Frequency distribution of isentropic stretching deformation (in $10^{-6}s^{-1}$) at the time of detection, $S_1$ (initial stretching), of each wave breaking event, for (a) $\Delta IPV_{detect} = 1$ PVU and (b) $\Delta IPV_{detect} = 1.7$ PVU.

as the center of the group passes by. In particular, the trough immediately to the west of the detected trough is split (by lag 1) in qualitatively the same manner as described above. This suggests that, in most individual cases, there is a percursory wave breaking event to the west of the detected one (see Fig. 4a for an example) which, however, does not fully develop as the center of the wave group progresses further eastward, in the sense that the associated wave does not completely propagate to the equatorward side of the jet; as it is the case for the finally detected major wave breaking event. This sequence of the successive occurrence of a precursory and a major wave breaking event closely resembles the two anticyclonically breaking waves over North America and the North Atlantic observed during the onset of the positive phase of the NAO (Benedict *et al.*, 2004, see their Fig. 3). Also the occurrence of the precursory event at a slightly higher latitude is in agreement with that observational study. In the course of the major wave breaking event, then, part of the wave activity is deposited on the equatorward side of the jet near a critical line and, consequently, the amplitude of the wave group reduces. Hence, no further AB-like wave breaking is found downstream of the wave breaking region.

In the according CB-composite, influenced by cyclonic background shear, the wave group shows poleward propagation. From the NW-SE tilted $IPV$ trough of the breaking wave a large scale cut-off low emerges at lag 0 and the corresponding cyclonic $IPV$ anomaly propagates further downstream along the jet. This behavior is well known also from cyclonic wave breaking events in idealized baroclinic wave life cycles. The most distinct feature of the cyclonically breaking event in the composite, however, appears to be the large scale and quasi-stationary anticyclonic $IPV$ anomaly at high relative latitudes, produced by poleward advection of low $IPV$ air. Moreover, this anomaly persists for about a week after the detection of the event. Furthermore, it is worth mentioning that a meridional dipole pattern with anticyclonic north of cyclonic $IPV$, being suggestive of the remnant of a blocking anomaly, is found in the wave breaking region already four days before the wave breaks. When during the subsequent days the wave group passes through that region, the wave breaking process appears to reinforce this preexisting pattern by generation of the anticyclonic $IPV$ anomaly, though the final anticyclonic anomaly occurs at sightly higher relative latitudes. Finally, in this composite neither the signature of NW-SE (or NE-SW) tilted troughs nor any other CB-like wave breaking event is found outside the wave breaking region, indicating wave propagation confined to a zonal wave guide on the eddy-driven jet. Hence, cyclonic wave breaking appears as a more zonally localized process and, additionally, the results suggest that CB events occur most likely in the region of a preexisting blocking pattern with an anticyclonic anomaly poleward of the jet, which is associated also with diffluent background flow (see absolute $IPV$ contours at lag -4). These characteristics resemble the single cyclonically breaking wave over the North Atlantic observed during the onset of the negative phase of the NAO (Benedict *et al.*, 2004, see their Fig. 5), and also captures some aspects known from simple models of positive synoptic eddy feedbacks on blocking anticyclones (Shutts, 1983; Illary, 1984; Haines and Marshall, 1987; Frisius *et al.*, 1998; Luo, 2005).

In summary, both AB- and CB-composites reveal the typical characteristics of anticyclonic and cyclonic synoptic scale wave breaking, respectively. We can further conclude that there is a distinct asymmetry between our AB- and CB-composites, in agreement with findings from AB- and CB-like wave breaking in idealized baroclinic wave life cycles. This asymmetry is characterized as follows: (i) While in the AB case the breaking wave quickly dissipates, the CB event produces a quasi-stationary and persistent anticyclonic anomaly at high relative latitudes. Accordingly, the average lifetimes of the events detected by the method



DOI: 10.1002/qj

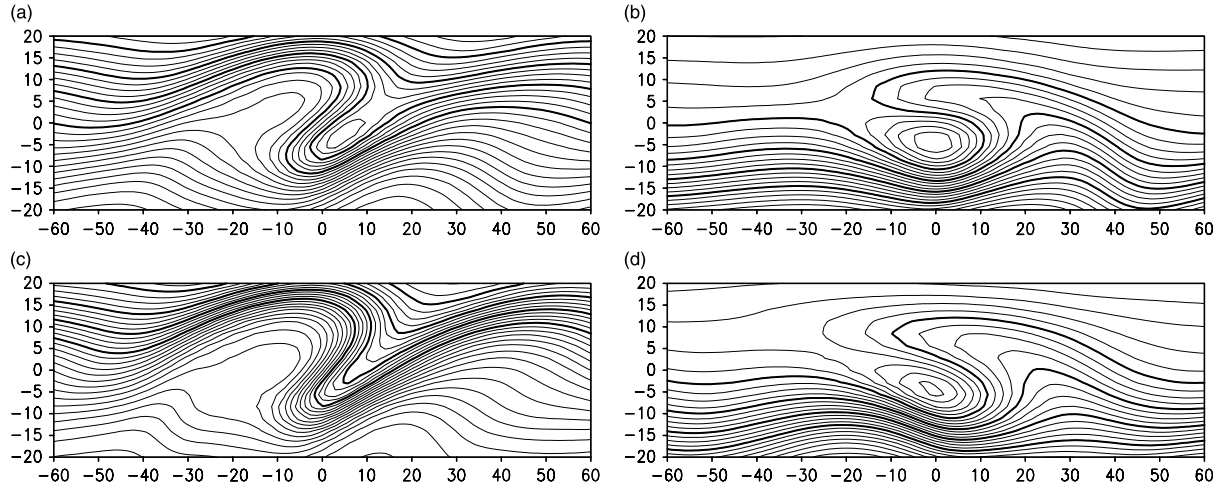


Figure 6. AB- (a, c) and CB-composites (b, d) of $IPV$ at $\theta = 320$ K (at the time of detection), using the threshold $S_1^\star = 26 \times 10^{-6}\mathrm{s}^{-1}$ (a, b) and the 15.9%-quantiles $S_1^{Q-}$ and $S_1^{Q+}$ (c, d) for classification into AB and CB. Contour interval is 0.125 PVU; thick contours are at 2, 2.5, 3 and 3.5 PVU. Coordinates are relative longitude and latitude.

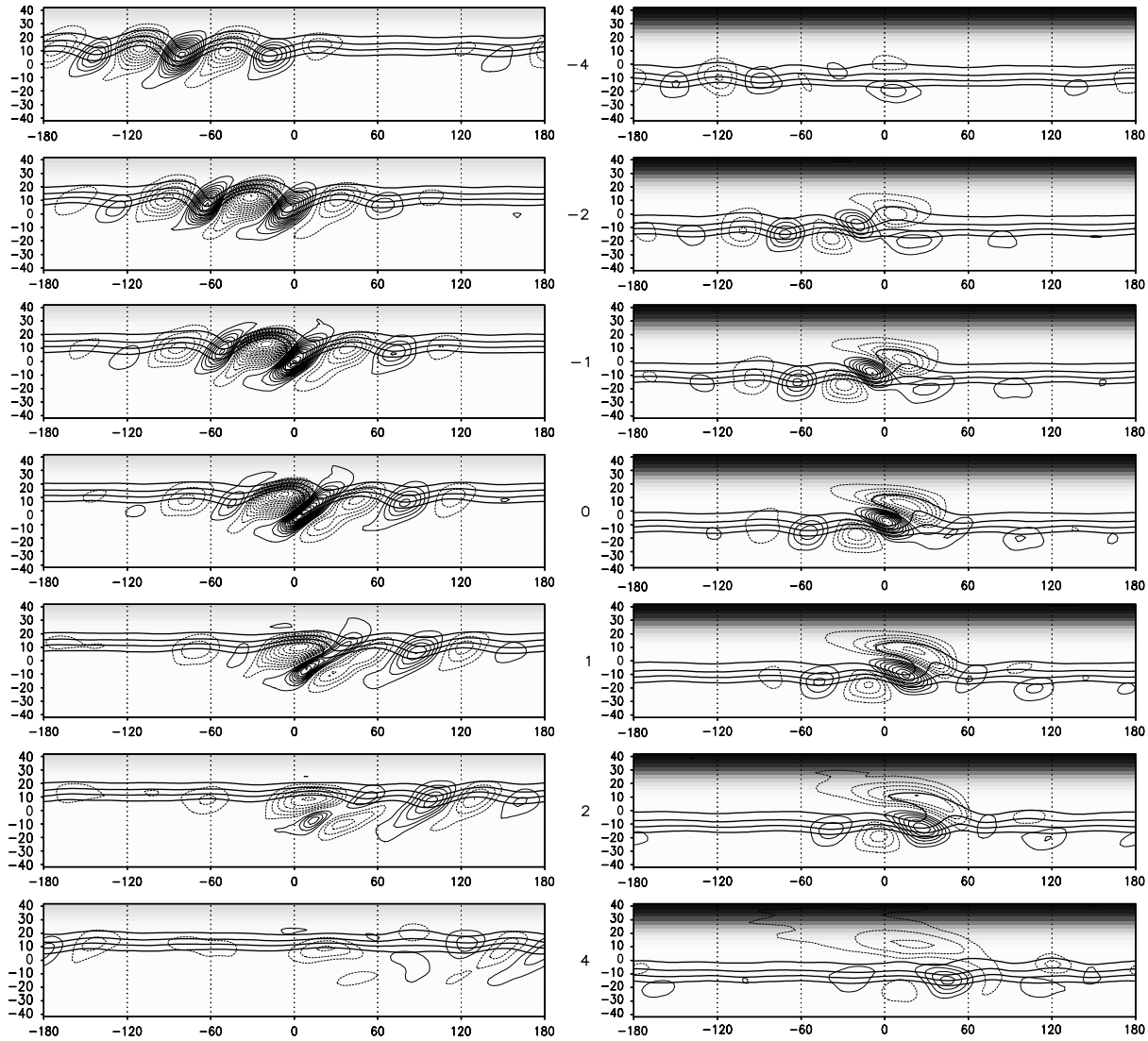


Figure 7. AB- (left) and CB-composite (right) of $IPV$ anomalies (with respect to zonal mean at lag -14 days) from lag -4 days to +4 days. Contour interval is 0.1 PVU, the zero contour is omitted, and dashed contours indicate negative values. Thick contours show total $IPV$ at 2, 2.5, 3 and 3.5 PVU. Coordinates are relative longitude and latitude. Relative latitudes which occurred for all (zero) events are shaded in white (black).



DOI: 10.1002/qj

are 2.6 days for AB and 4.3 days for CB. (ii) The AB-composite shows equatorward propagation of the entire wave group, whereas in the CB case poleward wave propagation occurs exclusively in a zonally confined region. (iii) CB-like wave breaking takes place preferably in a region of a preexisting diffluent pattern in the background flow, while AB events occur at an arbitrary longitude. The two latter points are consequences of the tendency to equatorward wave propagation due to the Earth's spherical geometry (e.g., Whitaker and Snyder, 1993) and also of the fact that wave breaking is generally facilitated by diffluent background flows (e.g., Peters and Waugh, 1996). Hence, the CB-composite reflects a situation where anticyclonic wave breaking is inhibited by a zonal wave guide, and isolated cyclonic wave breaking is triggered locally by background diffluence in the jet exit to the west of a preexisting blocking pattern.

### 4.2. Upper versus lower tropospheric flow evolution

Next, the upper tropospheric large scale flow evolution during AB and CB events is compared to that at lower tropospheric levels since significant differences are to be expected during baroclinic wave breaking processes. The evolution at upper levels is illustrated by composites of 300 hPa geopotential height, $z_{300}$, anomalies (Fig. 8) and, not surprisingly, similar structures are found as in the $IPV$ composite for the upper tropospheric $\theta$-surface. However, due to the scale and latitude dependent relation between PV and geopotential height some features are seen more clearly in the $z_{300}$ composite. Specifically, in the AB-composite the anticyclonic anomaly of the major AB event is found to dominate the upper tropospheric flow which, in turn, advects the northern (southern) part of the trough of the precursory (major) wave breaking event to its northern (southern) flank. Thus, at lag 2 a meridional tripole pattern is established rather than a clear positive phase NAO-like dipole. The according CB-composite highlights the reinforced preexisting blocking pattern which, at positive lags, closely resembles a stationary negative phase NAO-like dipole. Note, that the anticyclonic pole consists of a single stationary anticyclonic anomaly poleward of the jet, whereas the cyclonic pole is accounted for by eastward propagating cyclonic anomalies within the eddy-driven jet.

The evolution at lower levels, on the other hand, is presented in Fig. 9, showing composites of surface pressure anomalies. In the AB-composite at negative lags and western relative longitudes the cyclonic (anticyclonic) surface pressure anomalies propagate to higher (lower) latitudes during the life cycle of each individual wave as the wave group progresses eastward, reflecting the equatorward mass shift across the jet; as a consequence of the jet acceleration by eddy momentum fluxes caused by NE-SW tilted waves on its equatorward flank. Furthermore, since the eastward Rossby wave group velocity exceeds the phase velocity but also has an equatorward component, the corresponding anticyclones appear at successively lower latitudes as the wave group propagates to the equatorward side of the jet, where finally the major wave breaking event takes place and from which a strong positive phase NAO-like meridional surface pressure dipole emerges at lag 1. The south-eastern and southern flank of the associated anticyclones represents the anticyclonic branch of the shallow cold air outflow typically observed on the rear side of AB-like cyclones (see, e.g., Thorncroft *et al.*, 1993), while on the north-western and northern flank warm air advection takes place in the region of enhanced westerlies between the dipole centers. This thermal asymmetry of the surface anticyclones leads to the different structure at upper levels as seen in the tripole pattern in the $z_{300}$ composite (Fig. 8). Furthermore,

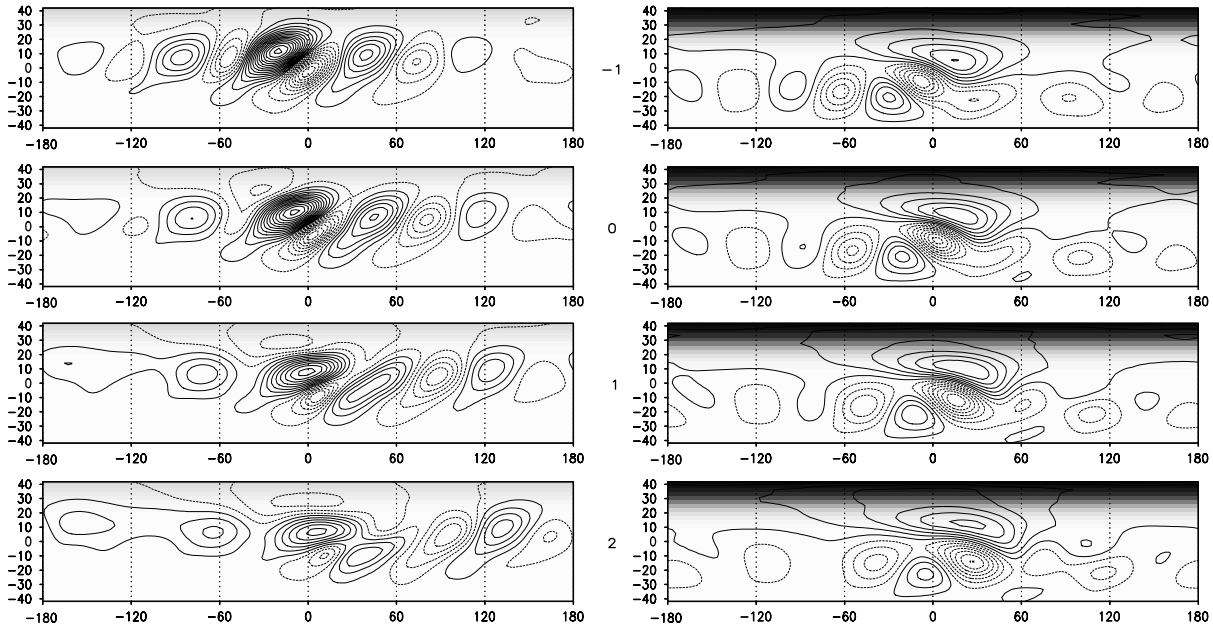


Figure 8. Same as Fig. 7, but for 300 hPa geopotential height anomalies from lag −1 day to +2 days, and the contour interval is 20 gpm (with contours at ..., −30, −10, 10, 30, ... gpm).



DOI: 10.1002/qj

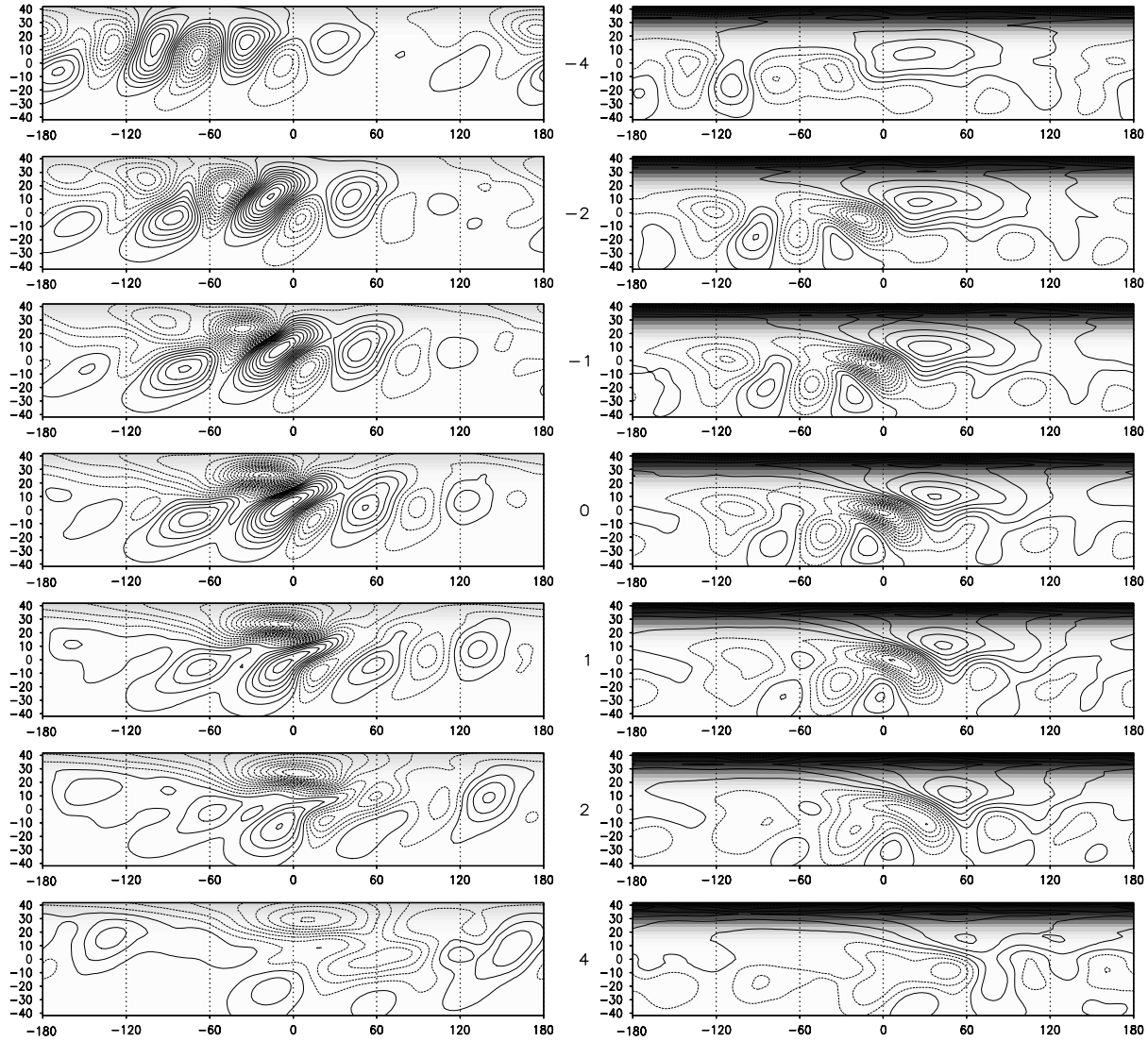


Figure 9. Same as Fig. 7, but for surface pressure anomalies, and the contour interval is 1 hPa (with contours at ..., −1.5, −0.5, 0.5, 1.5, ... hPa).

a surface cold-frontal cyclone is induced by the small cut-off low formed from the *IPV* trough above the surface cold air outflow of the major wave breaking event. Thus, this cyclonic anomaly confines the upper (lower) level anticyclonic anomaly at its southern (south-eastern) flank, compared to the observed anticyclonic anomaly during the positive phase NAO. During the subsequent days the surface pressure dipole pattern quickly decays as it is the case for the tripole pattern in the upper troposphere.

In the surface pressure CB-composite the preexisting blocking pattern is found at negative lags as in the upper troposphere. However, in contrast to the reinforcement of the high latitude anticyclone at upper tropospheric levels, the corresponding surface anticyclonic anomaly is largely deformed by the surface pressure cyclone of the breaking wave and is also moved eastward by about 45°, though it undergoes temporary amplification. Thus, there is no negative phase NAO-like surface pressure dipole generated by the CB event, unlike the upper tropospheric evolution. This surface pressure response is again understandable in terms of eddy momentum fluxes which (as for the anticyclonically breaking wave) locally accelerate the eastward zonal flow of the jet caused by the NW-SE tilted wave on its poleward flank. The resulting equatorward mass shift across the jet again leads to a negative (positive) surface pressure tendendy on the poleward (equatorward) flank of the jet (see lag -4 to lag 1 at zero relative longitude). The warm air advection on the leading edge (north-eastern flank) of the surface cyclone, however, helps to reinforce the upper tropospheric anticyclone above.

Summarizing this upper and lower tropospheric large scale flow evolution during AB and CB events we have shown that anticyclonic wave breaking as detected by our method drives a distinct positive phase NAO-like meridional circulation dipole at the surface but a different and more complex structure in the upper troposphere, while cyclonic wave breaking drives (and reinforces) a negative phase NAO-like dipole in the upper troposphere but not at the surface. Also the respective patterns of the response to AB events do not resemble those from CB events with opposite sign due to the distinct asymmetry



DOI: 10.1002/qj

between the dynamical evolution of AB and CB. And, furthermore, the respective response to cyclonic wave breaking appears to be more persistent than the response to anticyclonic wave breaking.

Hence, if the two kinds of wave breaking are, conceptually, thought to drive the different phases of the NAO, their respective contributions should lead to a threefold asymmetry of the NAO, specifically, in the horizontal, the vertical and in the temporal component. Observational evidence is given by Blessing *et al.* (2005). They find a temporal asymmetry between the two phases of the NAO with an average lifetime (daily NAO index above plus (below minus) one standard deviation of a principle component time series) of 3.3 days (4.5 days) for the positive (negative) phase. Note, that these average lifetimes of NAO events are very similar to the average wave breaking lifetime of 3.5 days (see section 3.3), and should not be compared directly to the autocorrelation time scale of the NAO of about ten days which, by contrast, is essentially a decay time scale. Any horizontal spatial asymmetry is naturally excluded by the conventionally used linear methods (EOF or correlation analysis) to define NAO indices, which are always based on a fixed spatial pattern.

Concerning the asymmetry in the vertical component it is important to note that, in spite of the differences between upper and lower levels, an NAO-like variability mode of equivalent barotropic structure may arise from the successive occurrence of AB and CB events. This is illustrated by the following idealized picture (Fig. 10): From a dynamical perspective the evolution of baroclinic wave life cycles, including wave breaking during their decay stage, should be viewed with reference to a state of increased baroclinic instability supporting baroclinic growth, rather than a time mean state. Such a baroclinically unstable state is characterized by increased vertical zonal wind shear, as indicated schematically by circles on the right hand side in Fig. 10, representing a vertical profile of zonal wind at a latitude that corresponds to the node of the NAO (left hand side in Fig. 10). Individual baroclinic waves grow under these conditions and will eventually break either anticyclonically or cyclonically during their barotropic decay stage that leads to a distinct reduction of baroclinic shear (indicated by thick lines in Fig. 10). In case of anticyclonic wave breaking a positive phase NAO-like circulation dipole is driven primarily at the surface associated with increased surface zonal winds at mid-latitudes, whereas cyclonic wave breaking drives a negative NAO-like circulation dipole confined mostly to the upper troposphere with reduced zonal winds (arrows labeled AB or CB in Fig. 10). Then, the successive occurrence of frequent wave breaking at some preferred location, like the North Atlantic storm-track region, will result in a variability pattern with respect to the time mean (indicated by thin dashed lines in Fig. 10) that resembles an equivalent barotropic NAO mode, although the response to each kind of wave breaking is highly asymmetric in the vertical with respect to the baroclinically unstable state. This implies that the difference between the respective patterns driven by AB and CB (thick lines in Fig. 10) may account for NAO-like variability rather than the individual responses. Certainly, additional investigations are necessary to further refine this highly idealized picture of the positive (negative) phase of the NAO being driven at lower (upper) levels. Specifically, a similar AB- and CB-composite analysis from zonally non-uniform simulations including an NAO-like variability mode at a fixed location or from observational data may allow for a close examination of these aspects by projecting the AB and CB responses onto the corresponding variability pattern.

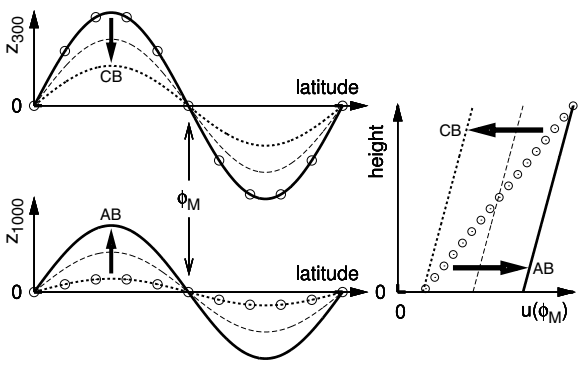


Figure 10. Schematic of equivalent barotropic NAO variability driven by AB (CB) at lower (upper) tropospheric levels. Meridional profile of geopotential height $z$ representing an NAO dipole at 1000 hPa and 300 hPa, and vertical profile of zonal wind $u$ between 1000 hPa and 300 hPa at latitude of maximum zonal winds $\phi_M$. From a baroclinically unstable state (circles), supporting baroclinic growth, either the positive (thick solid) or negative (thick dotted) NAO phase is driven by AB or CB, respectively, during the barotropic decay stage of a baroclinic life cycle. The time mean is represented by thin dashed lines.

Clearly, in the real atmosphere diffluent background flow by the quasi-stationary waves in the North Atlantic storm-track region is an important additional factor which favours and therefore localizes synoptic scale wave breaking there. Franzke *et al.* (2004) report that AB- and CB-like wave breaking in their model only occurs in the right location to drive NAO-like variability if a realistic zonally non-uniform basic state is chosen. However, still large case to case variability among individual wave breaking events is observed even in a localized storm-track. Thus, small scale structures of the composite wave breaking patterns (Figs. 7 to 9) would be smoothed out when averaging (in absolute longitude and latitude) a large ensemble of such events taking place in the North Atlantic storm-track region.

### 4.3. Further remarks: North Atlantic storm-track region

To conclude our synoptic interpretation, we may hypothesize to what extent other factors of the real North Atlantic storm-track region could modulate the response to anticyclonic and cyclonic wave breaking. First, in the AB-composite the upper tropospheric flow does not closely resemble the positive phase of the NAO due to the presence of the small cut-off low from the trough of the major wave breaking event (see lag 1 and lag 2). In a typical North Atlantic setting, however, this positive $IPV$ anomaly would be close to the onset of the subtropical jet over the eastern North Atlantic which can



DOI: 10.1002/qj

be expected to move that anomaly eastward and, thus, to allow for further southward extension of the dominant anticyclone at upper levels, inducing a more positive phase NAO-like pattern. Additionally, the northern cyclonic anomaly (from the precursory wave breaking event) might profit from the cold air reservoirs over Canada and Greenland in the sense that it is deepened by low level cold air advection.

And, second, in the CB case the upper tropospheric negative phase NAO-like pattern induced (and reinforced) by the cyclonically breaking wave might largely trigger zonally smaller scale blocking episodes over the same region, producing a significant negative phase NAO-like response at lower levels and the surface. Shabbar *et al.* (2001) present observational evidence of increased occurrence of North Atlantic blocking during the negative phase NAO, and Woollings *et al.* (2008) suggest an interpretation of the positive (negative) phase NAO being essentially the result of less (more) frequent blocking episodes. Their wave breaking index was indeed originally introduced as a blocking index by Pelly and Hoskins (2003). This suggests that their index captures a combination of CB events (in the light of baroclinic wave life cycles) and stationary blocking dipoles (in the sense of, e.g., Shutts, 1983) of smaller individual zonal scale than the negative phase NAO pattern itself. For individual real synoptic situations it might even be impossible to distinguish between these two concepts stemming from highly idealized model approaches. Note, that the strong forcing of positive phase NAO-like dipoles at the surface by anticyclonic wave breaking, however, is not made explicit by the Woollings *et al.* (2008) view.

### 4.4. Response of the annular mode

The zonally uniform forcing and boundary conditions of our model setup preclude the occurrence of any NAO-like variability mode at a zonally fixed location and, therefore, the quantitative analysis of its response to wave breaking events. However, observational and modeling evidence exists for the NAO being a zonally confined manifestation of the same dynamical processes that drive hemispheric scale variability modes like the Arctic Oscillation or the annular mode (Wallace, 2000; Ambaum *et al.*, 2001; Vallis *et al.*, 2004; Feldstein and Franzke, 2006). Thus, it is also reasonable to investigate the response of the annular mode to anticyclonic and cyclonic wave breaking. For this purpose the surface annular mode index (surface AMI) is calculated for each simulation separately by projection of daily zonal mean surface pressure fields (north of 20 °N) onto the first EOF pattern of monthly and zonal mean surface pressure fields. Accordingly, the 300 hPa AMI is constructed in the same way from 300 hPa geopotential height fields. Both indices are normalized by its standard deviation. The corresponding meridional annular mode structures are characterized by a maximum between 46 °N (Sim-0) and 49 °N (Sim-3) and minimum values north of 70 °N. Then, lagged AB- and CB-composites of the surface and the 300 hPa AMI are calculated, and shown in Fig. 11.

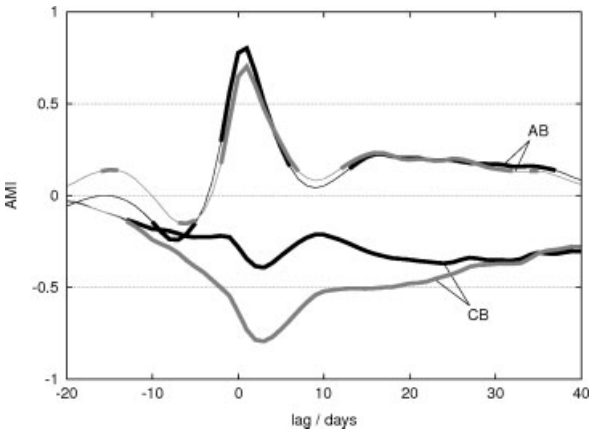


Figure 11. AB- and CB-composites (see labels) of the annular mode index at the surface (black lines) and at 300 hPa (gray lines). Thick lines indicate statistical significance at the 99.9% level.

Evidently, anticyclonic (cyclonic) wave breaking induces a significant positive (negative) response of the AMI, both at lower and upper tropospheric levels. The AMI peaks at lag 1 (lag 3) for AB (CB) and attains a value of 0.80 (-0.39) at the surface and 0.70 (-0.80) at 300 hPa. These results confirm the asymmetry of the response to AB and CB events in the temporal component and between lower and upper levels. While the surface AMI AB-composite exceeds, for example, 0.6 for only three days (lag 0 to lag 2), the 300 hPa AMI CB-composite is less than -0.6 for eight days (lag 0 to lag 7). For smaller absolute threshold values this temporal asymmetry is even more pronounced. Furthermore, the surface AMI CB-composite shows that cyclonic wave breaking rather ineffectively drives the negative phase of the annular mode at lower levels, in accordance with the finding that CB events do not produce a clear negative phase NAO-like dipole at the surface. However, the corresponding difference between the 300 hPa AMI AB-composites compared to that at the surface is smaller, although the synoptic signature of AB events at upper levels does not closely resemble the positive phase NAO. That this is due to the wider hemispheric extent of the AB signature at the peak time of the AMI can be seen in the respective AB- and CB-composites of surface pressure and 300 hPa geopotential height, with respect to the time mean (Fig. 12), now using absolute latitude and relative longitude. The 300 hPa AB-composite again (as in Fig. 8) exhibits a tripole pattern but large amplitude anticyclonic anomalies at mid-latitudes appear around the entire hemisphere (Fig. 12a), whereas the surface CB-composite (Fig. 12d) shows only weak cyclonic anomalies outside the wave breaking region, consistent with the more zonally confined nature of CB events.

It should also be mentioned that these composites reveal different dominant zonal wave numbers, with zonal wave number five for AB (see Fig. 12a) and wave number six for CB (see Fig. 12b). This is consistent with the result from idealized baroclinic wave life cycles that AB- (CB-) like behaviour is favoured for longer (shorter) synoptic waves (Hartmann and Zuercher, 1998; Orlanski,



DOI: 10.1002/qj

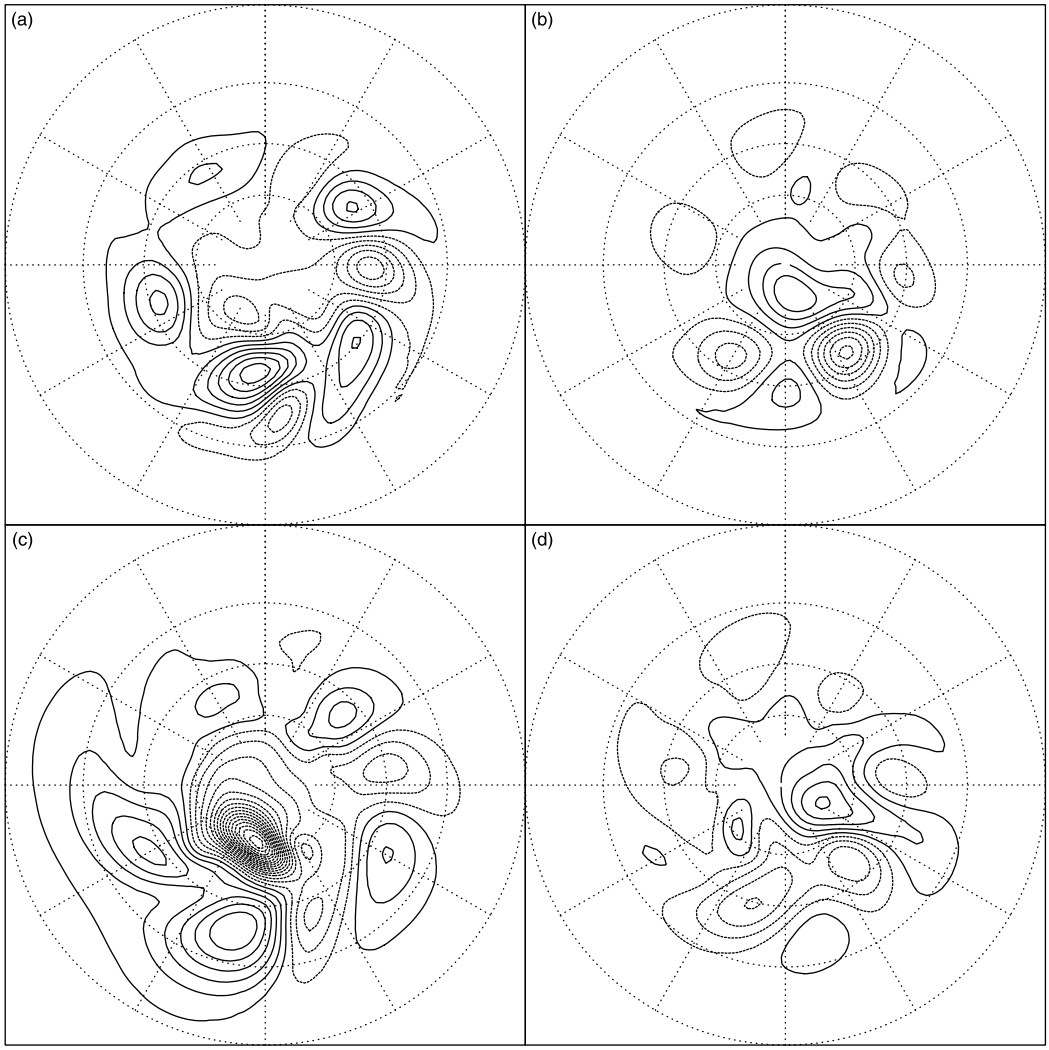


Figure 12. AB- (a, c) and CB-composites (b, d) of 300 hPa geopotential height (a, b) and surface pressure (c, d) anomalies (with respect to the time mean) at lag +1 day for AB- and +3 days for CB-composites. Contour intervals are the same as in Fig. 8 and Fig. 9. Coordinates are relative longitude and absolute latitude. Latitude circles are plotted at 0°, 20°, 40° and 60 °N.

2003; Wittman *et al.*, 2007), and with the study by Rivière and Orlanski (2007) who force a high-resolution model over the North Atlantic domain with observational data. Finally, we do not further interpret the weak but statistically significant AMI response to AB and CB at positive lags beyond about 10 days since this is likely to reflect the spurious and unrealistically long annular mode (decorrelation) time scale, which is typically found in semi-spectral simplified GCMs as the one used in this study, in particular, at the model resolution employed here (as shown, for example, by Gerber *et al.*, 2008). (The autocorrelation functions of the surface pressure AMI of our simulations have an *e*-folding time scale of 30 to 40 days, while in the real atmosphere time scales of order two weeks are observed.)

### 4.5. Influence of the stratosphere

As mentioned in section 2 the tropospheric eddy-driven jet shifts poleward as the stratospheric polar vortex is strengthened by diabatic cooling (Sim-0 to Sim-3). From the results of Polvani and Kushner (2002) and Kushner and Polvani (2004) it is highly suggestive that this jet shift arises from a baroclinic wave (or high-frequency synoptic scale) response in the troposphere projecting onto an internal tropospheric mode of variability which is characterized by meridional vacillation of the zonal mean eddy-driven jet (and is often associated with the tropospheric annular mode). This is particularly plausible since many observational and modeling studies indicate a strong interaction between mid-latitude high-frequency eddies and the tropospheric zonal mean zonal flow in the sense of a positive feedback that helps to maintain zonal flow anomalies by altered eddy propagation characteristics (e.g., Yu and Hartmann, 1993; Hartmann and Lo, 1998; Esler and Haynes, 1999; Lorenz and Hartmann, 2001).

In this eddy–zonal flow interaction framework the eddy feedback on the jet arises from eddy momentum fluxes associated with anomalous equatorward (poleward) high-frequency eddy propagation during a high (low) latitudinal position of the jet. It is, therefore, reasonable to ask whether this tendency to more equatorward (poleward)



DOI: 10.1002/qj

wave propagation in the presence of a higher (lower) latitudinal position of the jet is also reflected in our wave breaking statistics of the different simulations by more frequent AB (CB) events under a stronger (weaker) stratospheric polar vortex.

For this purpose we compare the distributions of the initial stretching $S_1$ of the different simulations (Fig. 13). The fraction of wave breaking events with small $S_1$ is largest for Sim-0 and reduces when the polar vortex is strengthened in Sim-1, Sim-2 and Sim-3, indicating more (less) frequent AB- (CB-) like behavior for a higher latitude tropospheric jet, below a stronger stratospheric jet. This is consistent with the observational result that the positive phase of the NAO as well as the Arcitc Oscillation/annular mode is favoured under strong stratospheric polar vortex conditions (Baldwin *et al.*, 1994; Thompson and Wallace, 1998; Baldwin and Dunkerton, 1999). Furthermore, the change of the ratio of the numbers of AB- to CB-like events is maximized, if the separation is made at $S_1^\star = 26 \times 10^{-6}\mathrm{s}^{-1}$. In section 3 this was shown to be a reasonable threshold value to distinguish between AB- and CB-like wave breaking (Fig. 6a, b) since it roughly separates the two modes in the $S_1$ frequency distribution (Fig. 5). The ratio then changes by 17% from Sim-0 to Sim-3 (see dotted line in Fig. 13).

Clearly, from this analysis it remains undecidable whether the stratospheric signal is mediated to the troposphere by direct modulation of tropospheric baroclinic waves penetrating into the lowermost stratospheric flow or by a zonal mean secondary circulation response to changed stratospheric wave forcing that induces the tropospheric jet shift which in turn influences the baroclinic waves and thus the synoptic scale wave breaking characteristics. However, the possibility of a direct response of baroclinic waves to lowermost stratospheric flow conditions is suggested by several modeling studies (Polvani and Kushner, 2002; Charlton *et al.*, 2004; Kushner and Polvani, 2004; Wittman *et al.*, 2004, 2007; Kunz *et al.*, 2009).

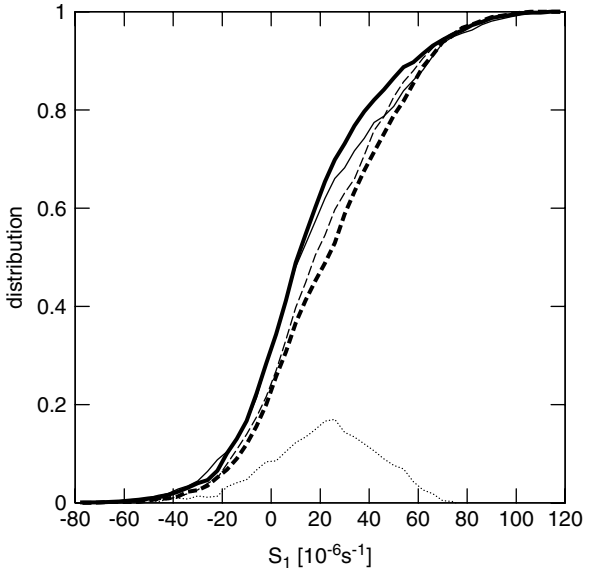


Figure 13. Distributions of isentropic stretching deformation (in $10^{-6}\mathrm{s}^{-1}$) at the time of detection, $S_1$ (initial stretching), of each wave breaking event from Sim-0 (thick solid), Sim-1 (thin solid), Sim-2 (thin dashed) and Sim-3 (thick dashed), and the difference Sim-0 minus Sim-3 (dotted).

Finally, in the context of the above discussion it should be noted that, as shown by Baldwin (2003), the observed tropospheric jet position is relatively insensitive to changes in the strength of the stratospheric polar vortex, in contrast to the above model results. However, this observational result does not affect the plausibility of our model setup since the zonal mean in Baldwin (2003) includes the Pacific sector and is also strongly influenced by the subtropical jet near 30 °N, whereas the jet in our model is more representative of the eddy-driven jet in the North Atlantic sector as discussed in section 2.

## 5. Discussion and conclusions

This idealized model study investigates the potential of synoptic scale anticyclonic and cyclonic wave breaking alone for driving the different phases of the NAO. A method for the detection of such wave breaking events is introduced and applied to four 25 years forced-dissipative simplified GCM simulations with perpetual northern winter conditions and zonally uniform forcing and boundary conditions.

The wave breaking detection method is based on the identification of reversals of the meridional $IPV$ gradient, and the horizontal stretching deformation field is used to classify the detected events into AB and CB. However, the chaotic nature of isentropic mixing due to mid-latitude synoptic eddies leads to a large variety of spatial $IPV$ patterns and, thus, many individual cases of wave breaking events exhibit a signature with aspects of both AB and CB behavior. Nevertheless, for strong $IPV$ reversals clear bimodality is found, suggesting that the concept of AB- and CB-like wave breaking, motivated by highly idealized adiabatic and frictionless baroclinic wave life cycle simulations with prescribed zonal wave number, is indeed also relevant for the case of wave groups in a forced-dissipative setup.

The long model time series (1200 months total) allows for composite analysis of only the most distinct AB and CB events (tails of $S_1$ frequency distribution). This immediately rises the question of the applicability of the method to observational data, say, reanalysis products (nowadays spanning over about 50 years), where the sample size is largely reduced to the order of 150 winter months. If, additionally, the analysis is confined to the North Atlantic sector, the expected number of wave breaking events is much less than 10% of the corresponding number in this study (4119 events total). Furthermore, the higher complexity of the real atmosphere flow due to stationary waves and also phenomena of smaller than the resolved scales in our model are expected to increase the case to case variability of wave breaking events, even if those fields are interpolated to T42 resolution. Nevertheless, the actual presence of frequent and clear AB- and CB-like signatures in observational tropopause charts



DOI: 10.1002/qj

and the appearance of anticyclonically and cyclonically breaking waves even in a composite analysis of the NAO (Benedict *et al.*, 2004) are promising for the successful application of the method to real atmosphere data, for the study of the effect of AB and CB events on low-frequency variability modes like the NAO or the Pacific North American (PNA) pattern.

The advantage of the idealized model setup used here, however, is the possibility to investigate the synoptic evolution of wave breaking in the absence of a stationary wave field, influences from the tropics or the surface. For this purpose AB- and CB-composites were presented. Regarding the question posed in the introduction of the potential of anticyclonic (cyclonic) wave breaking alone for driving positive (negative) phase NAO-like circulation dipoles we can draw the following main conclusions from our composite analysis:

- AB events are typically preceded by a precursory AB event (downstream development), resembling the evolution during the onset of the positive phase of the NAO, while cyclonic breaking occurs as a single CB event, as observed during the onset of the negative phase of the NAO (Benedict *et al.*, 2004), and is preferably triggered by a preexisting blocking (or negative phase NAO-like) pattern.
- AB events drive strong positive phase NAO-like dipoles at the surface but not at upper tropospheric levels due to the complex interaction of the precursory and the major wave breaking event, while CB events generate strong negative phase NAO-like dipoles at upper levels but not at the surface. (Note, that a single wave breaking event generally produces an anticyclonic PV anomaly north of a cyclonic anomaly. Therefore, for any cyclonic north of anticyclonic PV signature, as for the positive phase NAO, the interaction of two breaking waves is necessary. However, the resultant synoptic pattern does not need to be a simple meridional dipole; see AB-composites in section 4.)
- AB events are short-lived processes (average lifetime 2.6 days), while CB events persist for longer (4.3 days). This is true also for the response of the large scale flow (see previous point) and, thus, consistent with the observed asymmetry in the temporal component of the NAO (Blessing *et al.*, 2005).

Hence, anticyclonic (cyclonic) synoptic scale wave breaking is not capable of driving full positive (negative) phase NAO-like dipoles individually. Since, however, alternate forcing of a positive phase NAO-like dipole at the surface and a negative phase NAO-like dipole at upper levels would indeed generate NAO-like variability at either level, our results suggest that the successive occurrence of AB and CB events may drive an equivalent barotropic NAO-like variability mode in the troposphere. This picture of the positive (negative) phase NAO being driven by AB (CB) in the lower (upper) troposphere also explains the successful characterization of the NAO by Woollings *et al.* (2008) using a blocking index to capture (CB-like) wave breaking at the tropopause that drives the negative phase of the NAO, while in their view the positive phase of the NAO is represented by the absence of such upper tropospheric events. This suggests that the apparently different NAO–wave breaking views of Benedict *et al.* (2004) and Woollings *et al.* (2008) are indeed consistent.

Finally, more (less) frequent AB- (CB-) like behavior for a higher latitude tropospheric jet below a stronger stratospheric jet is found, consistent with the observed connection between the stratospheric polar vortex and the NAO as well as the Arctic Oscillation/annular mode. This issue is subject of a subsequent study including effects of quasi-stationary planetary waves which deeply extend into the stratosphere and, thereby, strongly support stratosphere troposphere interaction.

**Acknowledgements**

This work was funded by the Deutsche Forschungsgemeinschaft, project SFB-512. Discussion with Christian Franzke and Richard Greatbatch is greatly appreciated.

## A. Specification of equilibrium temperature

The equilibrium temperature $T_{Eq}$ is specified by:

$$T_{Eq}(\phi, p) = [1 - W(\phi, p)]T_{US}(p) + F_{trop}(p)T_{trop}(\phi) + [1-W(\phi, p)]T_{LS}(\phi, p) + W(\phi, p)T_{PV}(p), \quad (5)$$

where $\phi$ is latitude, $p$ is pressure and $T_{US}$ is the U.S. standard atmosphere (1976). $T_{Eq}(\phi, p)$ is transformed to the model $\sigma$-levels by $\sigma(p) = p/p_s$ with $p_s = 1013.25$ hPa. Tropospheric meridional temperature gradients are introduced by

$$T_{trop}(\phi) = \Delta T_{EP}\left((1/3) - \sin^2\phi\right) + \Delta T_{NS}\sin\phi \quad (6)$$

$$F_{trop}(p) = \begin{cases} 0 & \text{if } p < p_{trop} \\ \sin\left[(\pi/2)(p - p_{trop})/(p_s - p_{trop})\right] & \text{if } p \geq p_{trop}, \end{cases} \quad (7)$$

with $\Delta T_{EP} = 60$ K, $\Delta T_{NS} = -20$ K (northern winter), and $p_{trop}$ is the pressure level at 11 km in the U.S. standard atmosphere; and opposite meridional gradients in the lower stratosphere by

$$T_{LS}(\phi, p) = \begin{cases} \cos\left[(\pi/2)(p-p_{LS})/\Delta p_{LS}\right]\left(T_{LS}^{+} - \Delta T_{LS}\cos 2\phi\right) \\ \quad \ldots \text{if} \quad p_{LS} - \Delta p_{LS} \leq p \leq p_{LS} + \Delta p_{LS} \\ 0 \quad \text{otherwise}, \end{cases} \quad (8)$$



DOI: 10.1002/qj

where $p_{LS} = 100$ hPa, $\Delta p_{LS} = 90$ hPa, $\Delta T_{LS} = 15$ K and $T_{LS}^{+} = -5$ K. The stratospheric polar vortex is driven by high-latitude cooling in the stratosphere, as in Polvani and Kushner (2002). It takes the form

$$T_{PV}(p) = T_{US}(p_{PV})\,(p/p_{PV})^{\gamma R/g}\,, \tag{9}$$

which is an atmosphere with constant lapse rate $\gamma$, and is confined to polar latitudes by

$$W(\phi, p) = \begin{cases} (1/2)\left(1 + \tanh\left[\left(\phi - \phi_0\right)/\Delta\phi\right]\right) & \text{if} \quad p \le p_{PV} \\ 0 & \text{if} \quad p > p_{PV}, \end{cases} \tag{10}$$

with $\phi_0 = 50^\circ$, $\Delta\phi = 10^\circ$ and $p_{PV} = 100$ hPa. The value of $\gamma$ determines the strength of the stratospheric polar vortex forcing. For no polar vortex it is, additionally, $W(\phi, p) = 0$.

## References


Abatzoglou JT, Magnusdottir G. 2006. Opposing effects of reflective and nonreflective planetary wave breaking on the NAO. *J. Atmos. Sci.* **63**: 3448–3457.

Ambaum MHP, Hoskins BJ, Stephenson DB. 2001. Arctic oscillation or North Atlantic oscillation. *J. Climate* **14**: 3495–3507.

Appenzeller C, Davies HC. 1992. Structure of stratospheric intrusions into the troposphere. *Nature* **358**: 570–572.

Baldwin MP. 2003. Comment on "Tropospheric response to stratospheric perturbations in a relatively simple general circulation model" by Lorenzo M. Polvani and Paul J. Kushner. *Geophys. Res. Lett.* **30**: 1812, doi:10.1029/2003GL017 793.

Baldwin MP, Cheng X, Dunkerton TJ. 1994. Observed correlations between winter-mean tropospheric and stratospheric circulation anomalies. *Geophys. Res. Lett.* **21**: 1141–1144.

Baldwin MP, Dunkerton TJ. 1999. Propagation of the Arctic Oscillation from the stratosphere to the troposphere. *J. Geophys. Res.* **104**: 30 937–30 946.

Benedict JJ, Lee S, Feldstein SB. 2004. Synoptic view of the North Atlantic oscillation. *J. Atmos. Sci.* **61**: 121–144.

Blessing S, Fraedrich K, Junge M, Kunz T, Lunkeit F. 2005. Daily North-Atlantic oscillation (NAO) index: statistics and its stratospheric polar vortex dependence. *Meteorol. Zeitschrift* **14**: 763–769.

Charlton AJ, O'Neill A, Lahoz WA, Massacand AC. 2004. Sensitivity of tropospheric forecasts to stratospheric initial conditions. *Q. J. R. Meteorol. Soc.* **130**: 1771–1792.

Esler JG, Haynes PH. 1999. Baroclinic wave breaking and the internal variability of the tropospheric circulation. *J. Atmos. Sci.* **56**: 4014–4031.

Feldstein SB. 2000. The timescale, power spectra, and climate noise properties of teleconnection patterns. *J. Climate* **13**: 4430–4440.

Feldstein SB. 2003. The dynamics of NAO teleconnection pattern growth and decay. *Q. J. R. Meteorol. Soc.* **129**: 901–924.

Feldstein SB, Franzke C. 2006. Are the North Atlantic oscillation and the northern annular mode distinguishable? *J. Atmos. Sci.* **63**: 2915–2930.

Fraedrich K, Kirk E, Luksch U, Lunkeit F. 2005. The portable university model of the atmosphere (PUMA): Storm track dynamics and low-frequency variability. *Meteorol. Zeitschrift* **14**: 735–745.

Fraedrich K, Kirk E, Lunkeit F. 1998. Portable University Model of the Atmosphere. Technical Report 16, DKRZ.

Franzke C, Lee S, Feldstein SB. 2004. Is the North Atlantic oscillation a breaking wave? *J. Atmos. Sci.* **61**: 145–160.

Frisius T, Lunkeit F, Fraedrich K, James IA. 1998. Storm-track organization and variability in a simplified atmospheric global circulation model (SGCM). *Q. J. R. Meteorol. Soc.* **124**: 1019–1043.

Gerber EP, Voronin S, Polvani LM. 2008. Testing the annular mode autocorrelation timescale in simple atmospheric general circulation models. *Mon. Weath. Rev.* **136**: 1523–1536.

Haines K, Marshall JC. 1987. Eddy-forced coherent structures as a prototype of atmospheric blocking. *Q. J. R. Meteorol. Soc.* **113**: 681–704.

Hartmann DL, Lo F. 1998. Wave-driven zonal flow vacillation in the southern hemisphere. *J. Atmos. Sci.* **55**: 1303–1315.

Hartmann DL, Zuercher P. 1998. Response of baroclinic life cycles to barotropic shear. *J. Atmos. Sci.* **55**: 297–313.

Held IM, Suarez MJ. 1994. A proposal for the intercomparison of the dynamical cores of atmospheric general circulation models. *Bull. Amer. Meteor. Soc.* **75**: 1825–1830.

Hurrell JW. 1995. Decadal trends in the North Atlantic oscillation: Regional temperatures and precipitation. *Science* **269**: 676–679.

Hurrell JW, Kushnir Y, Ottersen G, Visbeck M (eds). 2003. The North Atlantic oscillation: Climate significance and environmental impact. Geophys. Monogr., vol. 134. Amer. Geophys. Union. 279pp.

Illary L. 1984. A diagnostic study of the potential vorticity in a warm blocking anticyclone. *J. Atmos. Sci.* **41**: 3518–3526.

Kunz T, Fraedrich K, Lunkeit F. 2009. Response of baroclinic wave life cycles to stratospheric flow conditions. *J. Atmos. Sci.* In press.

Kushner PJ, Polvani LM. 2004. Stratosphere-troposphere coupling in a relatively simple AGCM: The role of eddies. *J. Climate* **17**: 629–639.

Lorenz DJ, Hartmann DL. 2001. Eddy-zonal flow feedback in the southern hemisphere. *J. Atmos. Sci.* **58**: 3312–3327.

Luo D. 2005. A barotropic envelope Rossby soliton model for block-eddy interaction. Part I: Effect of topography. *J. Atmos. Sci.* **62**: 5–21.

Martius O, Schwierz C, Davies HC. 2007. Breaking waves at the tropopause in the wintertime northern hemisphere: Climatological analyses of the orientation and the theoretical LC1/2 classification. *J. Atmos. Sci.* **64**: 2576–2592.

McIntyre ME, Palmer TN. 1983. Breaking planetary waves in the stratosphere. *Nature* **305**: 593–600.

McIntyre ME, Palmer TN. 1985. A note on the general concept of wave breaking for Rossby and gravity waves. *Pure Appl. Geophys.* **123**: 964–975.

Nakamura M, Plumb RA. 1994. The effects of flow asymmetry on the direction of Rossby wave breaking. *J. Atmos. Sci.* **51**: 2031–2045.

Orlanski I. 2003. Bifurcation of eddy life cycles: Implications for storm track variability. *J. Atmos. Sci.* **60**: 993–1023.

Pelly JL, Hoskins BJ. 2003. A new perspective on blocking. *J. Atmos. Sci.* **60**: 743–755.

Peters D, Waugh DW. 1996. Influence of barotropic shear on the poleward advection of upper-tropospheric air. *J. Atmos. Sci.* **53**: 3013–3031.

Polvani LM, Kushner PJ. 2002. Tropospheric response to stratospheric perturbations in a relatively simple general circulation model. *Geophys. Res. Lett.* **29**: 1114, doi:10.1029/2001GL014 284.

Rivière G, Orlanski I. 2007. Characteristics of the Atlantic storm-track activity and its relation with the North Atlantic oscillation. *J. Atmos. Sci.* **64**: 241–266.

Scinocca JF, Haynes PH. 1998. Dynamical forcing of stratospheric planetary waves by tropospheric baroclinic eddies. *J. Atmos. Sci.* **55**: 2361–2392.

Shabbar A, Huang J, Higuchi K. 2001. The relation between the wintertime North Atlantic oscillation and blocking episodes in the North Atlantic. *Int. J. Climatol.* **21**: 355–369.

Shutts GJ. 1983. The propagation of eddies in diffluent jetstreams: eddy vorticity forcing of 'blocking' flow fields. *Q. J. R. Meteorol. Soc.* **109**: 737–761.

Thompson DWJ, Wallace JM. 1998. The Arctic Oscillation signature in the wintertime geopotential height and temperature fields. *Geophys. Res. Lett.* **25**: 1297–1300.

Thorncroft CD, Hoskins BJ. 1990. Frontal cyclogenesis. *J. Atmos. Sci.* **47**: 2317–2336.

Thorncroft CD, Hoskins BJ, McIntyre ME. 1993. Two paradigms of baroclinic-wave life-cycle behaviour. *Q. J. R. Meteorol. Soc.* **119**: 17–55.

Vallis GK, Gerber EP, Kushner PJ, Cash BA. 2004. A mechanism and simple dynamical model of the North Atlantic oscillation and annular modes. *J. Atmos. Sci.* **61**: 264–280.

Wallace JM. 2000. North Atlantic oscillation/annular mode: Two paradigms-one phenomenon. *Q. J. R. Meteorol. Soc.* **126**: 791–805.

Waugh DW, Plumb RA, Atkinson RJ, Schoeberl MR, Lait LR, Newman PA, Loewenstein M, Webster CR, May RD. 1994. Transport of material out of the stratospheric Arctic vortex through Rossby wave breaking. *J. Geophys. Res.* **99**: 1071–1088.

Whitaker JS, Snyder C. 1993. The effects of spherical geometry on the evolution of baroclinic waves. *J. Atmos. Sci.* **50**: 597–612.

Wittman MAH, Charlton AJ, Polvani LM. 2007. The effect of lower stratospheric shear on baroclinic instability. *J. Atmos. Sci.* **64**: 479–496.

Wittman MAH, Polvani LM, Scott RK, Charlton AJ. 2004. Stratospheric influence on baroclinic lifecycles and its connection to the Arctic Oscillation. *Geophys. Res. Lett.* **31**: L16 113, doi:10.1029/2004GL020 503.

Woollings T, Hoskins B, Blackburn M, Berrisford P. 2008. A new Rossby wavebreaking interpretation of the North Atlantic oscillation. *J. Atmos. Sci.* **65**: 609–626.

Yu JY, Hartmann DL. 1993. Zonal flow vacillation and eddy forcing in a simple GCM of the atmosphere. *J. Atmos. Sci.* **50**: 3244–3259.